Analysis and optimization of the generalized Schwarz method for elliptic problems with application to fluid–structure interaction

Giacomo Gigante · Christian Vergara

Received: 12 December 2013 / Revised: 6 November 2014 Published online: 04 December 2014

1 Introduction

The Optimized Schwarz Method (OSM) is a domain decomposition method based on the splitting of the computational domain into subdomains, on the linear combination of the interface conditions between subdomains through the introduction of interface operators, and on the search of optimized interface operators in a proper subset (e.g. the constants) which guarantee good convergence properties [20,25].

G. Gigante · C. Vergara (✉)
Dipartimento di Ingegneria Gestionale, dell'Informazione e della Produzione,
Università degli Studi di Bergamo, Viale Marconi 5, 24044 Dalmine, BG, Italy
e-mail: christian.vergara@unibg.it

G. Gigante
e-mail: giacomo.gigante@unibg.it

This method has been considered so far for many problems in the case of flat interfaces, such as the advection–reaction–diffusion problem [15,21], the Helmholtz equation [16,26], the shallow-water equations [32], the Maxwell's equations [7], the fluid–structure interaction problem [17] and the scattering problem [33]. Recently, in [18] OSM has been considered and analyzed for the reaction–diffusion problem in the case of cylindrical interfaces.

In this work, we consider a general framework to analyze OSM for linear ellip-tic problems. This will allow to consider several situations, namely the case of flat, cylindrical and spherical interfaces, in any dimension. This is done by applying a general Fourier transform to the linear elliptic problem allowing to obtain a synthetic expression of this equation covering all the cited cases, and to write explicitly its solution.

Once we have derived a general expression for the solution of the elliptic problem, we provide the exact convergence set of the interface symbols for the generalized Schwarz method, that is the iterative algorithm obtained for general, non-optimized interface operators. Then, we propose a new optimization strategy, based on looking for optimized constant interface values along a selected curve in the space of the parameters, which is supposed to lead to good convergence properties. This allows to obtain an optimization problem with respect to one scalar parameter and to write explicitly a range of such a parameter which guarantees that the reduction factor is below a given value.

Finally, we apply the proposed analysis and optimization procedure to the fluid–structure interaction (FSI) problem, obtaining new estimates for the interface parameters. We present also some 3D numerical results both in a simplified and in a real geometry inspired by the haemodynamic applications.

The outline of this work is as follows. In Sect. 2 we present the general solution of the linear elliptic problem, whereas in Sect. 3 we provide the exact convergence set of the interface symbols. In Sect. 4 we present the new optimization procedure, and in Sects. 5.1 and 5.2 we show two applications of our strategies to problems introduced so far in the literature. In Sect. 5.3 we apply our results to the FSI problem, and finally in Sect. 6 we present the numerical results.

2 General solution of the elliptic problem

In this section we provide a general discussion about the solution of a linear elliptic problem. In particular, let n be a positive integer, and d an integer between 1 and n. Let Ω be a subset of $\mathbb{R}^n$ of the form

$$\Omega := \{(\boldsymbol{x}, \boldsymbol{y}) : \boldsymbol{x} \in \mathbb{R}^d\,,\, a < \|\boldsymbol{x}\| < b, \boldsymbol{y} \in \mathbb{R}^{n-d}\},$$

where $d \geq 2$ and $0 \leq a < b \leq +\infty$. In the case $d = 1$, we set

$$\Omega := \{(x, \boldsymbol{y}) : a < x < b, \boldsymbol{y} \in \mathbb{R}^{n-1}\},$$

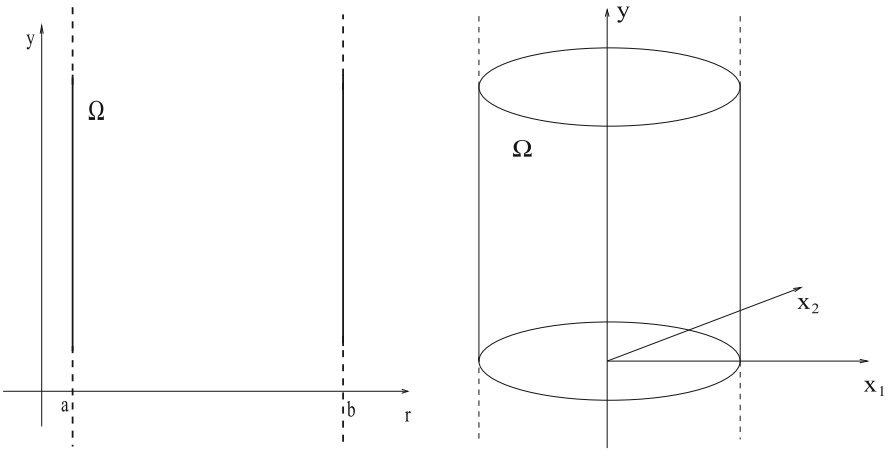

Fig. 1 Possible domain configurations. *Left* $n = 2,\ d = 1$, *right* $n = 3,\ d = 2$

so that $\boldsymbol{x}$ is a real number and we will assume $-\infty \leq a < b \leq +\infty$. For example, if $n = 3$, Ω is a spherical shell when $d = 3$, a cylindrical shell when $d = 2$, and a "thick vertical wall" when $d = 1$, whereas if $n = 2$, Ω is a circular crown for $d = 2$ and a vertical stripe for $d = 1$, see Fig. 1.

Given a function u, we will use the following notation:

$$\Delta_{\boldsymbol{x}} u(\boldsymbol{x}, \boldsymbol{y}) = \sum_{j=1}^{d} \frac{\partial^2 u}{\partial x_j^2}(\boldsymbol{x}, \boldsymbol{y}), \quad \Delta_{\boldsymbol{y}} u(\boldsymbol{x}, \boldsymbol{y}) = \sum_{j=1}^{n-d} \frac{\partial^2 u}{\partial y_j^2}(\boldsymbol{x}, \boldsymbol{y}),$$

$$\nabla_{\boldsymbol{x}} u(\boldsymbol{x}, \boldsymbol{y}) = \left(\frac{\partial u}{\partial x_1}(\boldsymbol{x}, \boldsymbol{y}), \ldots, \frac{\partial u}{\partial x_d}(\boldsymbol{x}, \boldsymbol{y}) \right)^T,$$

$$\nabla_{\boldsymbol{y}} u(\boldsymbol{x}, \boldsymbol{y}) = \left(\frac{\partial u}{\partial y_1}(\boldsymbol{x}, \boldsymbol{y}), \ldots, \frac{\partial u}{\partial y_{n-d}}(\boldsymbol{x}, \boldsymbol{y}) \right)^T.$$

With this notation, given $\mu > 0,\ \xi \in \mathbb{R}$ and $\boldsymbol{\beta} \in \mathbb{R}^n$, we can introduce the operator $\mathcal{L}$ as follows

$$\mathcal{L}u = -\mu \Delta u + \boldsymbol{\beta} \cdot \nabla u + \xi u = -\mu \Delta_{\boldsymbol{x}} u - \mu \Delta_{\boldsymbol{y}} u + \boldsymbol{\beta}_{\boldsymbol{x}} \cdot \nabla_{\boldsymbol{x}} u + \boldsymbol{\beta}_{\boldsymbol{y}} \cdot \nabla_{\boldsymbol{y}} u + \xi u,$$

where $\boldsymbol{\beta} = (\boldsymbol{\beta}_{\boldsymbol{x}}, \boldsymbol{\beta}_{\boldsymbol{y}})$, with $\boldsymbol{\beta}_{\boldsymbol{x}} = (\beta_1, \ldots, \beta_d)$ and $\boldsymbol{\beta}_{\boldsymbol{y}} = (\beta_{d+1}, \ldots, \beta_n)$. Throughout the paper we will assume $\boldsymbol{\beta}_{\boldsymbol{x}} = \mathbf{0}$, so that the operator reduces to

$$\mathcal{L}u = -\mu \Delta_{\boldsymbol{x}} u - \mu \Delta_{\boldsymbol{y}} u + \boldsymbol{\beta}_{\boldsymbol{y}} \cdot \nabla_{\boldsymbol{y}} u + \xi u.$$

We want now to write an explicit expression of the solution of the equation $\mathcal{L}u = 0$. Due to the particular shape of Ω, it is natural to write the Laplacian $\Delta_{\boldsymbol{x}}$ in terms of the d-dimensional spherical coordinates. Thus, when $d \geq 2$, writing $\boldsymbol{x} = r\,\boldsymbol{x}'$, where $r = \|\boldsymbol{x}\|$ and $\boldsymbol{x}' = \boldsymbol{x}/\|\boldsymbol{x}\|$, we have (see, e.g., [11], Lemmas 2.62 and 2.63)

$$\Delta_{\boldsymbol{x}} u(r\boldsymbol{x}', \boldsymbol{y}) = \frac{\partial^2 u}{\partial r^2}(r\boldsymbol{x}', \boldsymbol{y}) + \frac{d-1}{r}\frac{\partial u}{\partial r}(r\boldsymbol{x}', \boldsymbol{y}) + \frac{1}{r^2}(\Delta_{S^{d-1}} u(r\bullet, \boldsymbol{y}))(\boldsymbol{x}'), \quad (1)$$

where $\Delta_{S^{d-1}}$ is the Laplace–Beltrami operator on the $d-1$-dimensional sphere

$$S^{d-1} = \{\boldsymbol{x} \in \mathbb{R}^d : \|\boldsymbol{x}\| = 1\}.$$

If instead $d = 1$, we call r the variable $\boldsymbol{x}$ and we simply have

$$\Delta_{\boldsymbol{x}} u = \frac{\partial^2 u}{\partial r^2}.$$

Now, let

$$\{P_{m,l}(\boldsymbol{x}')\}_{m=0,l=1}^{+\infty,k_m}$$

be an orthonormal basis of spherical harmonics of the sphere S^{d-1}, where k_m is the dimension of the eigenspace associated with the eigenvalue λ_m, whose expression is given by $\lambda_m = m(m+d-2)$, $m = 0, \ldots, +\infty$, see, e.g., [11], Corollary 2.55. We have $k_m = (2m+d-2)\frac{(m+d-3)!}{m!(d-2)!}$, which in the case $d = 2$ leads to $k_m = 2$ for any m. Then, for any function $u(\boldsymbol{x}, \boldsymbol{y})$, let

$$\widehat{u}(r, m, l, \boldsymbol{k}) = \int_{\mathbb{R}^{n-d}} \left(\int_{S^{d-1}} u(r\boldsymbol{x}', \boldsymbol{y}) \overline{P_{m,l}(\boldsymbol{x}')} d\sigma(\boldsymbol{x}') \right) e^{-i\boldsymbol{y}\cdot\boldsymbol{k}} d\boldsymbol{y} \quad (2)$$

be its Fourier transform with respect to $\boldsymbol{x}'$ and $\boldsymbol{y}$. Notice that the frequency variable $\boldsymbol{k}$ related to the spatial variable $\boldsymbol{y}$ is continuous, whereas the frequency variable m related to the spatial variable $\boldsymbol{x}'$ is discrete, since S^{d-1} is a compact manifold.

Applying the transform (2) to (1), we obtain

$$\begin{aligned}\widehat{\Delta_{\boldsymbol{x}} u}(r, m, l, \boldsymbol{k}) = {} & \frac{\partial^2 \widehat{u}}{\partial r^2}(r, m, l, \boldsymbol{k}) + \frac{d-1}{r}\frac{\partial \widehat{u}}{\partial r}(r, m, l, \boldsymbol{k}) \\ & - \frac{m(m+d-2)}{r^2}\widehat{u}(r, m, l, \boldsymbol{k}),\end{aligned}$$

and then

$$\begin{aligned}&\widehat{\mathcal{L}u}(r, m, l, \boldsymbol{k}) \\ &= -\mu \left(\frac{\partial^2 \widehat{u}}{\partial r^2}(r, m, l, \boldsymbol{k}) + \frac{d-1}{r}\frac{\partial \widehat{u}}{\partial r}(r, m, l, \boldsymbol{k}) - \frac{m(m+d-2)}{r^2}\widehat{u}(r, m, l, \boldsymbol{k}) \right) \\ &\quad + \|\boldsymbol{k}\|^2 \mu\, \widehat{u}(r, m, l, \boldsymbol{k}) - i\boldsymbol{\beta}_{\boldsymbol{y}} \cdot \boldsymbol{k}\, \widehat{u}(r, m, l, \boldsymbol{k}) + \xi\, \widehat{u}(r, m, l, \boldsymbol{k}).\end{aligned}$$

Then, the equation $\mathcal{L} = 0$ becomes

$$\frac{\partial^2 \widehat{u}}{\partial r^2} + \frac{d-1}{r}\frac{\partial \widehat{u}}{\partial r} - \left(\frac{m(m+d-2)}{r^2} + \alpha^2 \right) \widehat{u} = 0, \quad (3)$$

where

$$\alpha = \left(\|\boldsymbol{k}\|^2 + \frac{\xi}{\mu} - i \frac{\boldsymbol{\beta}_y}{\mu} \cdot \boldsymbol{k} \right)^{1/2}$$

where $\gamma^{1/2}$ is the square root of $\gamma \in \mathbb{C}$ satisfying the condition $0 \leq \arg(\gamma) < \pi$. Of course, if $d = n$, the Fourier transform in the variable $\boldsymbol{y}$ disappears and we have to take $\boldsymbol{k} = \boldsymbol{0}$, so that $\alpha = \left(\frac{\xi}{\mu}\right)^{1/2}$ and the Eq. (3) becomes

$$\frac{\partial^2 \widehat{u}}{\partial r^2} + \frac{d-1}{r} \frac{\partial \widehat{u}}{\partial r} - \left(\frac{m(m+d-2)}{r^2} + \frac{\xi}{\mu} \right) \widehat{u} = 0.$$

Notice that we considered homogeneous forcing term since in the convergence analyses reported in the next sections we will analyze without loss of generality the convergence to the zero solution. Observe also that the equation $\mathcal{L} = 0$ needs to be equipped with suitable boundary conditions on $\partial\Omega$, see Sect. 3. Finally, we notice that in the case $d = 2$ (cylindrical domain for $n = 3$) Eq. (3) is exactly the one discussed in [18] whose solutions are the modified Bessel functions, see Sect. 2.2.

2.1 Solution of the case $d = 1$

When $d = 1$, the Fourier transform in the variable $\boldsymbol{x}'$ disappears and in (3) we have to take $m = 0$, obtaining

$$\frac{\partial^2 \widehat{u}}{\partial r^2} - \alpha^2 \widehat{u} = 0.$$

If $\alpha \neq 0$, the solutions of this equation are simply

$$\widehat{u}(r, \boldsymbol{k}) = X_1(\boldsymbol{k}) e^{\alpha r} + X_2(\boldsymbol{k}) e^{-\alpha r},$$

for suitable functions X_1 and X_2 determined by the boundary conditions. In particular, if $\boldsymbol{\beta}_y = \boldsymbol{0}$, we have

$$\widehat{u}(r, \boldsymbol{k}) = X_1(\boldsymbol{k}) e^{r\left(\|\boldsymbol{k}\|^2 + \frac{\xi}{\mu}\right)^{1/2}} + X_2(\boldsymbol{k}) e^{-r\left(\|\boldsymbol{k}\|^2 + \frac{\xi}{\mu}\right)^{1/2}}.$$

If $\xi > 0$, then $\|\boldsymbol{k}\|^2 + \frac{\xi}{\mu} > 0$ and the solutions are

$$\widehat{u}(r, \boldsymbol{k}) = X_1(\boldsymbol{k}) e^{r\sqrt{\|\boldsymbol{k}\|^2 + \frac{\xi}{\mu}}} + X_2(\boldsymbol{k}) e^{-r\sqrt{\|\boldsymbol{k}\|^2 + \frac{\xi}{\mu}}},$$

where we have used the symbol $\sqrt{\gamma}$ to indicate the square root of a real non-negative number γ. If, on the contrary, $\xi \leq 0$, then we have three possibilities, according to $\|\boldsymbol{k}\|$:

$$\widehat{u}(r,\boldsymbol{k}) = \begin{cases} X_1(\boldsymbol{k})e^{r\sqrt{\|\boldsymbol{k}\|^2+\frac{\xi}{\mu}}} + X_2(\boldsymbol{k})e^{-r\sqrt{\|\boldsymbol{k}\|^2+\frac{\xi}{\mu}}} & \text{if } \|\boldsymbol{k}\|^2 > -\frac{\xi}{\mu}, \\ X_1(\boldsymbol{k}) + X_2(\boldsymbol{k})r & \text{if } \|\boldsymbol{k}\|^2 = -\frac{\xi}{\mu}, \\ X_1(\boldsymbol{k})\cos\left(r\sqrt{-\|\boldsymbol{k}\|^2-\frac{\xi}{\mu}}\right) & \\ \quad +X_2(\boldsymbol{k})\sin\left(r\sqrt{-\|\boldsymbol{k}\|^2-\frac{\xi}{\mu}}\right) & \text{if } \|\boldsymbol{k}\|^2 < -\frac{\xi}{\mu}. \end{cases}$$

2.2 Solution of the case $d > 1$

The equation in this case is (3). If $\alpha \neq 0$, with the change of variables

$$\widehat{u}(r) = v(\alpha r)r^{-\frac{d-2}{2}},$$

this equation becomes

$$v''(t) + \frac{1}{t}v'(t) - \left(1 + \frac{\left(m+\frac{d-2}{2}\right)^2}{t^2}\right)v(t) = 0.$$

This is the modified Bessel equation, and the solutions are

$$v(t) = {}_2X_1 I_{m+\frac{d-2}{2}}(t) + {}_2X_2 K_{m+\frac{d-2}{2}}(t),$$

where I_ν and K_ν are the modified Bessel functions, see [23]. Thus, we have

$$\widehat{u}(r,m,l,\boldsymbol{k}) = X_1(m,l,\boldsymbol{k})\frac{I_{m+\frac{d-2}{2}}(\alpha r)}{r^{\frac{d-2}{2}}} + X_2(m,l,\boldsymbol{k})\frac{K_{m+\frac{d-2}{2}}(\alpha r)}{r^{\frac{d-2}{2}}}. \tag{4}$$

Once again, let us look closely to the case $\boldsymbol{\beta_y} = \mathbf{0}$, so that $\alpha = (\|\boldsymbol{k}\|^2 + \frac{\xi}{\mu})^{1/2}$. If $\xi > 0$, then $\alpha = \sqrt{\|\boldsymbol{k}\|^2 + \frac{\xi}{\mu}}$ and the solutions are

$$\begin{aligned}\widehat{u}(r,m,l,\boldsymbol{k}) = {} & X_1(m,l,\boldsymbol{k})\frac{I_{m+\frac{d-2}{2}}\left(r\sqrt{\|\boldsymbol{k}\|^2+\frac{\xi}{\mu}}\right)}{r^{\frac{d-2}{2}}} \\ & + X_2(m,l,\boldsymbol{k})\frac{K_{m+\frac{d-2}{2}}\left(r\sqrt{\|\boldsymbol{k}\|^2+\frac{\xi}{\mu}}\right)}{r^{\frac{d-2}{2}}}.\end{aligned}$$

If, on the contrary, $\xi \leq 0$, then we have three possibilities, according to $\|\boldsymbol{k}\|$:
if $\|\boldsymbol{k}\|^2 > -\frac{\xi}{\mu}$, then

$$\begin{aligned}\widehat{u}(r,m,l,\boldsymbol{k}) = {} & X_1(m,l,\boldsymbol{k})\frac{I_{m+\frac{d-2}{2}}\left(r\sqrt{\|\boldsymbol{k}\|^2+\frac{\xi}{\mu}}\right)}{r^{\frac{d-2}{2}}} \\ & + X_2(m,l,\boldsymbol{k})\frac{K_{m+\frac{d-2}{2}}\left(r\sqrt{\|\boldsymbol{k}\|^2+\frac{\xi}{\mu}}\right)}{r^{\frac{d-2}{2}}};\end{aligned}$$

if $\|\boldsymbol{k}\|^2 = -\frac{\xi}{\mu}$, then

$$\begin{aligned}\widehat{u}(r,m,l,\boldsymbol{k}) &= X_1(m,l,\boldsymbol{k})\frac{r^{m+\frac{d-2}{2}}}{r^{\frac{d-2}{2}}} + X_2(m,l,\boldsymbol{k})\frac{r^{-\left(m+\frac{d-2}{2}\right)}}{r^{\frac{d-2}{2}}}\\ &= X_1(m,l,\boldsymbol{k})r^m + X_2(m,l,\boldsymbol{k})r^{-d-m+2};\end{aligned}$$

if $\|\boldsymbol{k}\|^2 < -\frac{\xi}{\mu}$, then

$$\begin{aligned}\widehat{u}(r,m,l,\boldsymbol{k}) = X_1(m,l,\boldsymbol{k})&\frac{J_{m+\frac{d-2}{2}}\left(r\sqrt{-\|\boldsymbol{k}\|^2-\frac{\xi}{\mu}}\right)}{r^{\frac{d-2}{2}}}\\ &+X_2(m,l,\boldsymbol{k})\frac{Y_{m+\frac{d-2}{2}}\left(r\sqrt{-\|\boldsymbol{k}\|^2-\frac{\xi}{\mu}}\right)}{r^{\frac{d-2}{2}}}.\end{aligned}$$

Observe that in the case $\|\boldsymbol{k}\|^2 < -\frac{\xi}{\mu}$, in order to avoid complications due to the presence of complex valued functions, we have taken a different expression than the one coming from (4), based on the introduction of the Bessel functions J_ν and Y_ν, see [23].
In all the cases considered in the previous two subsections, the solution of (3) has the general form

$$\widehat{u}(r,m,l,\boldsymbol{k}) = X_1(m,l,\boldsymbol{k})g_1(r,m,\boldsymbol{k}) + X_2(m,l,\boldsymbol{k})g_2(r,m,\boldsymbol{k}). \tag{5}$$

for suitable functions X_1 and X_2 determined by the boundary conditions.

3 Convergence analysis of the generalized Schwarz method

For any real number L, $a \le L \le b$, let Σ_L be defined by

$$\Sigma_L := \{(\boldsymbol{x},\boldsymbol{y}) : \boldsymbol{x} \in \mathbb{R}^d,\ \|\boldsymbol{x}\| = L,\ \boldsymbol{y} \in \mathbb{R}^{n-d}\}.$$

This is a surface for $n = 3$ and a curve for $n = 2$. We fix now a real number R, $a < R < b$. Then, Σ_R divides Ω into two non-overlapping subdomains, namely

$$\begin{aligned}\Omega_1 &:= \{(\boldsymbol{x},\boldsymbol{y}) : \boldsymbol{x} \in \mathbb{R}^d,\ a < \|\boldsymbol{x}\| < R,\ \boldsymbol{y} \in \mathbb{R}^{n-d}\},\\ \Omega_2 &:= \{(\boldsymbol{x},\boldsymbol{y}) : \boldsymbol{x} \in \mathbb{R}^d,\ R < \|\boldsymbol{x}\| < b,\ \boldsymbol{y} \in \mathbb{R}^{n-d}\},\end{aligned}$$

see Fig. 2. In particular, we have the following cases: $n = 2$, $d = 1$, straight line interface; $n = 3$, $d = 1$, plane interface; $n = 2$, $d = 2$, circular interface; $n = 3$, $d = 2$, cylindrical interface; $n = 3$, $d = 3$, spherical interface.

We suppose that the domain Ω is subdivided into the two non-overlapping subdomains Ω_1 and Ω_2. Then, we consider the following coupled problem:

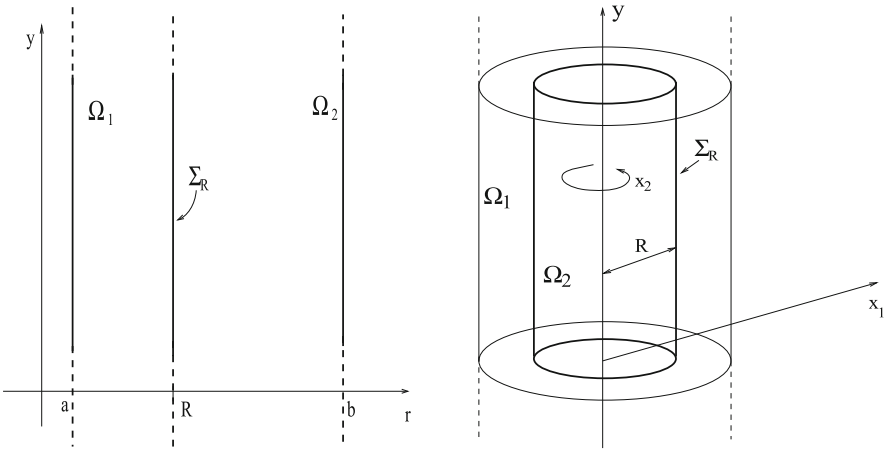

Fig. 2 Possible splitting of the domain. *Left* $n = 2,\ d = 1$, *right* $n = 3,\ d = 2$

$$
\begin{cases}
\mathcal{L}_1 u_1 = 0 & (\boldsymbol{x}, \boldsymbol{y}) \in \Omega_1, \\
\gamma_1 u_1 + \mu_1 \dfrac{\partial u_1}{\partial r} = 0 & (\boldsymbol{x}, \boldsymbol{y}) \in \Sigma_a, \\
u_1 = \delta u_2 + (1-\delta)\kappa_D \mu_2 \dfrac{\partial u_2}{\partial r} & (\boldsymbol{x}, \boldsymbol{y}) \in \Sigma_R, \\
\mu_1 \dfrac{\partial u_1}{\partial r} = \delta \mu_2 \dfrac{\partial u_2}{\partial r} + (1-\delta)\kappa_N u_2 & (\boldsymbol{x}, \boldsymbol{y}) \in \Sigma_R, \\
\gamma_2 u_2 + \mu_2 \dfrac{\partial u_2}{\partial r} = 0 & (\boldsymbol{x}, \boldsymbol{y}) \in \Sigma_b, \\
\mathcal{L}_2 u_2 = 0 & (\boldsymbol{x}, \boldsymbol{y}) \in \Omega_2,
\end{cases}
\tag{6}
$$

where $\mathcal{L}_i := -\mu_i \, \Delta + \boldsymbol{\beta}_i \cdot \nabla \; + \; \xi_i$, $i = 1, 2$, μ_i, $\boldsymbol{\beta}_i$, ξ_i, γ_i are constant within each subdomain, but they could in principle assume different values in the two subdomains,
$\kappa_D, \kappa_N \in \mathbb{R}$ account for possible heterogeneous couplings, $\delta = 0,\ 1$, and $\partial/\partial r$ is the directional derivative with respect to the outward unit normal to Σ_a, Σ_R or Σ_b. In the case $\delta = 1$, the interface conditions $(6)_{3-4}$ state the continuity of $u = (u_1,\ u_2)$ and of the tractions. whereas the case $\delta = 0$ arises for example when coupling the Darcy problem with the wave equation, see Sect. 5.3. We observe also that we prescribed Robin conditions on the physical boundaries Σ_a and Σ_b, to make the discussion as general as possible. If $d < n$, Ω_1 and Ω_2 are unbounded in the $\boldsymbol{y}$ directions, so that we require that the corresponding solution decays for $\| \boldsymbol{y}\| \to +\infty$. Analogously, if Ω_1 and/or Ω_2 are unbounded in the $\boldsymbol{x}$ directions, that is if $d = 1$ and $a = -\infty$, or $b = +\infty$, we again require that the corresponding solution decays at infinity ($\gamma_i = +\infty$). When $d \geq 2$ and $a = 0$, condition $(6)_2$ on Σ_a should be replaced with

$$
\int_{\mathbb{R}^{n-d}} \int_{S^{d-1}} |u_1(r\boldsymbol{x}', \boldsymbol{y})| d\sigma(\boldsymbol{x}') d\boldsymbol{y} \quad \text{bounded as} \;\; r \to 0^+. \tag{7}
$$

By linearly combining the interface conditions $(6)_{3-4}$, through the linear operators $\mathcal{S}_i$, $i = 1,\ 2$, acting in the tangential direction to Σ_R, we obtain the following equivalent coupled problem [9,25]:

$$
\begin{cases}
\mathcal{L}_1 u_1 = 0 & (\boldsymbol{x}, \boldsymbol{y}) \in \Omega_1, \\
\gamma_1 u_1 + \mu_1 \dfrac{\partial u_1}{\partial r} = 0 & (\boldsymbol{x}, \boldsymbol{y}) \in \Sigma_a, \\
\mathcal{S}_1 u_1 + \mu_1 \dfrac{\partial u_1}{\partial r} = \delta \mathcal{S}_1 u_2 + (1-\delta)\mathcal{S}_1 \kappa_D \mu_2 \dfrac{\partial u_2}{\partial r} + \delta \mu_2 \dfrac{\partial u_2}{\partial r} & \\
\quad + (1-\delta)\kappa_N u_2 & (\boldsymbol{x}, \boldsymbol{y}) \in \Sigma_R, \\
\delta \mathcal{S}_2 u_2 + (1-\delta)\mathcal{S}_2 \kappa_D \mu_2 \dfrac{\partial u_2}{\partial r} + \delta \mu_2 \dfrac{\partial u_2}{\partial r} + (1-\delta)\kappa_N u_2 & \\
\quad = \mathcal{S}_2 u_1 + \mu_1 \frac{\partial u_1}{\partial r} & (\boldsymbol{x}, \boldsymbol{y}) \in \Sigma_R, \\
\gamma_2 u_2 + \mu_2 \dfrac{\partial u_2}{\partial r} = 0 & (\boldsymbol{x}, \boldsymbol{y}) \in \Sigma_b, \\
\mathcal{L}_2 u_2 = 0 & (\boldsymbol{x}, \boldsymbol{y}) \in \Omega_2.
\end{cases} \tag{8}
$$

To solve problem (8) we consider the following *generalized Schwarz method* at iteration j:

$$
\begin{cases}
\mathcal{L}_1 u_1^j = 0 & (\boldsymbol{x}, \boldsymbol{y}) \in \Omega_1, \\
\gamma_1 u_1^j + \dfrac{\partial u_1^j}{\partial r} = 0 & (\boldsymbol{x}, \boldsymbol{y}) \in \Sigma_a, \\
\mathcal{S}_1 u_1^j + \mu_1 \dfrac{\partial u_1^j}{\partial r} & \\
= \delta \mathcal{S}_1 u_2^{j-1} + (1-\delta)\mathcal{S}_1 \kappa_D \mu_2 \dfrac{\partial u_2^{j-1}}{\partial r} + \delta \mu_2 \dfrac{\partial u_2^{j-1}}{\partial r} & \\
\quad + (1-\delta)\kappa_N u_2^{j-1} & (\boldsymbol{x}, \boldsymbol{y}) \in \Sigma_R, \\
\mathcal{L}_2 u_2^j = 0 & (\boldsymbol{x}, \boldsymbol{y}) \in \Omega_2, \\
\gamma_2 u_2^j + \mu_2 \dfrac{\partial u_2^j}{\partial r} = 0 & (\boldsymbol{x}, \boldsymbol{y}) \in \Sigma_b \\
\delta \mathcal{S}_2 u_2^j + (1-\delta)\mathcal{S}_2 \kappa_D \mu_2 \dfrac{\partial u_2^j}{\partial r} + \delta \mu_2 \dfrac{\partial u_2^j}{\partial r} + (1-\delta)\kappa_N u_2^j & \\
\quad = \mathcal{S}_2 u_1^j + \mu_1 \frac{\partial u_1^j}{\partial r} & (\boldsymbol{x}, \boldsymbol{y}) \in \Sigma_R.
\end{cases} \tag{9}
$$

By applying the transform (2) to the previous iterations and thanks to the boundary conditions, the solution of each of the two equations in (9) has the general form of (5), that is

$$
\widehat{u_i}^j(r, m, l, \boldsymbol{k}) = X_i^j(m, l, \boldsymbol{k})\, g_i(r, m, \boldsymbol{k}), \quad i = 1, 2, \tag{10}
$$

for suitable functions X_i^j and g_i. Then, we have the following results.

Proposition 1 *Let*

$$
\begin{aligned}
A(m, \boldsymbol{k}) &:= \frac{-\delta \mu_2 \frac{\partial g_2}{\partial r}(R, m, \boldsymbol{k}) - (1-\delta)\kappa_N g_2(R, m, \boldsymbol{k})}{\delta g_2(R, m, \boldsymbol{k}) + (1-\delta)\kappa_D \mu_2 \frac{\partial g_2}{\partial r}(R, m, \boldsymbol{k})}, \\
B(m, \boldsymbol{k}) &:= -\frac{\mu_1}{g_1(R, m, \boldsymbol{k})} \frac{\partial g_1}{\partial r}(R, m, \boldsymbol{k}).
\end{aligned} \tag{11}
$$

Then, the reduction factor related to iterations (9) *is given by*

$$\rho(m,l,\boldsymbol{k}) = \left| \frac{\sigma_1(m,l,\boldsymbol{k}) - A(m,\boldsymbol{k})}{\sigma_2(m,l,\boldsymbol{k}) - A(m,\boldsymbol{k})} \cdot \frac{\sigma_2(m,l,\boldsymbol{k}) - B(m,\boldsymbol{k})}{\sigma_1(m,l,\boldsymbol{k}) - B(m,\boldsymbol{k})} \right|, \tag{12}$$

where σ_i *are the symbols related to the operators* $\mathcal{S}_i$, $i = 1, 2$.

Proof We start by noticing that the reduction factor could be defined as $\rho = \left| \frac{X_2^j}{X_2^{j-1}} \right|$, see, e.g., [15]. After the application of the Fourier transform to problem (9), we have that the interface conditions $(9)_{3,6}$ read as follows:

$$\begin{aligned}
&\sigma_1 \widehat{u_1}^j(R) + \mu_1 \frac{\partial \widehat{u_1}^j}{\partial r}(R) \\
&\quad = (\delta\sigma_1 + (1-\delta)\kappa_N)\widehat{u_2}^{j-1}(R) + ((1-\delta)\sigma_1\kappa_D + \delta)\mu_2 \frac{\partial \widehat{u_2}^{j-1}}{\partial r}(R), \\
&(\delta\sigma_2 + (1-\delta)\kappa_N)\widehat{u_2}^j(R) + ((1-\delta)\sigma_2\kappa_D + \delta)\mu_2 \frac{\partial \widehat{u_2}^j}{\partial r}(R) \\
&\quad = \sigma_2 \widehat{u_1}^j(R) + \mu_1 \frac{\partial \widehat{u_1}^j}{\partial r}(R).
\end{aligned}$$

Then, substituting the solutions (10) into the above interface conditions and eliminating X_1^j, the thesis easily follows. □

In the following result, we provide the exact convergence sets for the symbols σ_1 and σ_2.

Theorem 1 *Fix* m *and* $\boldsymbol{k}$. *Then, under the assumption* $A > B$, *with* A *and* B *given by* (11), *the inequality*

$$|\rho(m,l,\boldsymbol{k})| = \left| \frac{\sigma_1(m,l,\boldsymbol{k}) - A(m,\boldsymbol{k})}{\sigma_2(m,l,\boldsymbol{k}) - A(m,\boldsymbol{k})} \cdot \frac{\sigma_2(m,l,\boldsymbol{k}) - B(m,\boldsymbol{k})}{\sigma_1(m,l,\boldsymbol{k}) - B(m,\boldsymbol{k})} \right| < 1 \tag{13}$$

holds if and only if $(\sigma_1, \sigma_2) \in \Theta(A, B) := \Theta_1(A, B) \cup \Theta_2(A, B)$, *where*

$$\begin{aligned}
\Theta_1(A,B) &= \left\{ (\sigma_1,\sigma_2) : \sigma_2 < \sigma_1 \text{ and } \left(\sigma_1 - \tfrac{A+B}{2}\right)\left(\sigma_2 - \tfrac{A+B}{2}\right) < \left(\tfrac{B-A}{2}\right)^2 \right\}, \\
\Theta_2(A,B) &= \left\{ (\sigma_1,\sigma_2) : \sigma_2 > \sigma_1 \text{ and } \left(\sigma_1 - \tfrac{A+B}{2}\right)\left(\sigma_2 - \tfrac{A+B}{2}\right) > \left(\tfrac{B-A}{2}\right)^2 \right\}.
\end{aligned} \tag{14}$$

Furthermore, $|\rho| = 0$ *if and only if* $\sigma_1(m,l,\boldsymbol{k}) = \sigma_1^{opt}(m,\boldsymbol{k}) := A(m,\boldsymbol{k})$ *and* $\sigma_2(m,l,\boldsymbol{k}) \neq A(m,\boldsymbol{k})$, *or* $\sigma_2(m,l,\boldsymbol{k}) = \sigma_2^{opt}(m,\boldsymbol{k}) := B(m,\boldsymbol{k})$ *and* $\sigma_1(m,l,\boldsymbol{k}) \neq B(m,\boldsymbol{k})$, *whereas* $|\rho| = 1$ *if and only if* $(\sigma_1,\sigma_2) \in \partial\Theta(A,B)\backslash\{(A,A),(B,B)\}$.

Proof Inequality (13) can be rewritten as

$$\begin{aligned}
&|(\sigma_1 - A)(\sigma_2 - B)| < |(\sigma_1 - B)(\sigma_2 - A)|, \\
&|\sigma_1\sigma_2 - A\sigma_2 - B\sigma_1 + AB| < |\sigma_1\sigma_2 - A\sigma_1 - B\sigma_2 + AB|.
\end{aligned}$$

Now, by analyzing the sign of the two terms, we have that the above inequality becomes

$$\begin{cases} (A-B)(\sigma_1-\sigma_2) < 0 \\ \qquad\qquad \text{if } (\sigma_1-A)(\sigma_2-B) \geq 0 \text{ and } (\sigma_1-B)(\sigma_2-A) > 0, \\ 2\sigma_1\sigma_2 - (A+B)\sigma_1 - (A+B)\sigma_2 + 2AB < 0 \\ \qquad\qquad \text{if } (\sigma_1-A)(\sigma_2-B) \geq 0 \text{ and } (\sigma_1-B)(\sigma_2-A) < 0, \\ 2\sigma_1\sigma_2 - (A+B)\sigma_1 - (A+B)\sigma_2 + 2AB > 0 \\ \qquad\qquad \text{if } (\sigma_1-A)(\sigma_2-B) < 0 \text{ and } (\sigma_1-B)(\sigma_2-A) > 0, \\ (A-B)(\sigma_1-\sigma_2) > 0 \\ \qquad\qquad \text{if } (\sigma_1-A)(\sigma_2-B) < 0 \text{ and } (\sigma_1-B)(\sigma_2-A) < 0. \end{cases}$$

By exploiting the assumption $A > B$, we obtain

$$\begin{cases} \sigma_1-\sigma_2 < 0 \quad \text{if } \sigma_1 \geq A,\ \sigma_2 > A \text{ or } \sigma_1 < B,\ \sigma_2 \leq B, \\ 2\sigma_1\sigma_2 - (A+B)\sigma_1 - (A+B)\sigma_2 + 2AB < 0 \\ \qquad\qquad \text{if } B \leq \sigma_2 < A, \sigma_1 \geq A \text{ or } B < \sigma_1 \leq A,\ \sigma_2 \leq B, \\ 2\sigma_1\sigma_2 - (A+B)\sigma_1 - (A+B)\sigma_2 + 2AB > 0 \\ \qquad\qquad \text{if } B < \sigma_2 < A, \sigma_1 < B \text{ or } B < \sigma_1 < A,\ \sigma_2 > A, \\ \sigma_1-\sigma_2 > 0 \quad \text{if } \sigma_1 > A,\ \sigma_2 < B \text{ or } \sigma_1 < B,\ \sigma_2 > A, \text{ or } B < \sigma_1, \sigma_2 < A. \end{cases} \tag{15}$$

Now, if $\sigma_2 < \sigma_1$ the above reduces to

$$\begin{cases} \sigma_1-\sigma_2 < 0 \quad \text{if } \sigma_1 > \sigma_2 > A, \text{ or } \sigma_2 < \sigma_1 < B, \\ 2\sigma_1\sigma_2 - (A+B)\sigma_1 - (A+B)\sigma_2 + 2AB < 0 \\ \qquad\qquad \text{if } B \leq \sigma_2 < A, \sigma_1 \geq A \text{ or } B < \sigma_1 \leq A,\ \sigma_2 \leq B, \\ \sigma_1-\sigma_2 > 0 \quad \text{if } \sigma_1 > A,\ \sigma_2 < B, \text{or } B < \sigma_2 < \sigma_1 < A, \end{cases}$$

or equivalently

$$\begin{cases} 2\sigma_1\sigma_2 - (A+B)\sigma_1 - (A+B)\sigma_2 + 2AB < 0 \\ \qquad\qquad \text{if } B \leq \sigma_2 < A, \sigma_1 \geq A \text{ or } B < \sigma_1 \leq A,\ \sigma_2 \leq B, \\ \text{any } (\sigma_1, \sigma_2) \\ \qquad\qquad \text{if } \sigma_1 > A,\ \sigma_2 < B, \text{or } B < \sigma_2 < \sigma_1 < A. \end{cases}$$

This is equivalent to require $(\sigma_1, \sigma_2) \in \Theta_1(A, B)$ defined in $(14)_1$. If $\sigma_2 > \sigma_1$, analogous steps, starting from (15), lead to require $(\sigma_1, \sigma_2) \in \Theta_2(A, B)$ defined in $(14)_2$. This concludes the first part of the Theorem. The second part of the Theorem follows straightforwardly.

Remark 1 We observe that Θ_1 and Θ_2 defined in (14) are limited by the line $\sigma_1 = \sigma_2$ and by the hyperbola

$$\left(\sigma_1 - \frac{A+B}{2}\right)\left(\sigma_2 - \frac{A+B}{2}\right) = \left(\frac{B-A}{2}\right)^2,$$

see Fig. 3. Since the latter curve depends on m and $\boldsymbol{k}$, we have that also the regions Θ_1 and Θ_2 depend on m and $\boldsymbol{k}$.

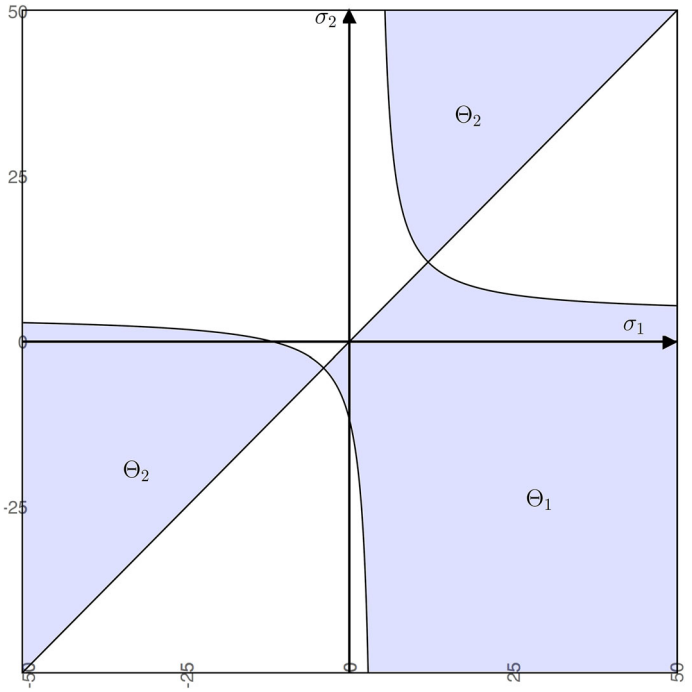

Fig. 3 Convergence set $\Theta(A, B)$ given by (14) (in *blue*) for the particular choice $A = 12$, $B = -4$ (color figure online)

We also observe that $|\rho| = 1$ for $(\sigma_1, \sigma_2) \in \partial\Theta(A, B) \setminus \{(A, A), (B, B)\}$ and for $(\sigma_1, \sigma_2) \to \infty$ inside $\Theta(A, B)$.

In the next result, we provide a better characterization of the regions Θ_1 and Θ_2.

Lemma 1 *Fix m and* $\boldsymbol{k}$. *If* $0 < \theta < 1$, *then the level sets*

$$\left|\frac{\sigma_1 - A}{\sigma_2 - A}\frac{\sigma_2 - B}{\sigma_1 - B}\right| = \theta \tag{16}$$

are the hyperbolae

$$\left(\sigma_1 - M - \frac{1+\theta}{1-\theta}D\right)\left(\sigma_2 - M + \frac{1+\theta}{1-\theta}D\right) = -\frac{4\theta}{(1-\theta)^2}D^2,$$
$$\left(\sigma_1 - M - \frac{1-\theta}{1+\theta}D\right)\left(\sigma_2 - M + \frac{1-\theta}{1+\theta}D\right) = \frac{4\theta}{(1+\theta)^2}D^2,$$

where

$$M = \frac{A+B}{2}, \quad D = \frac{A-B}{2}.$$

For a given θ, the above hyperbolae, restricted to $\Theta_1(A, B)$, delimit a region $\Theta_{1,\theta}(A, B)$, containing the point (A, B), where

$$\left|\frac{\sigma_1 - A}{\sigma_2 - A}\frac{\sigma_2 - B}{\sigma_1 - B}\right| \leq \theta. \tag{17}$$

More precisely

$$\Theta_{1,\theta}(A, B) = \Theta_\theta^{++}(A, B) \cup \Theta_\theta^{--}(A, B) \cup \Theta_\theta^{+-}(A, B) \cup \Theta_\theta^{-+}(A, B),$$

where

$$\begin{aligned}
\Theta_\theta^{++}(A, B) = \Bigg\{ & (\sigma_1, \sigma_2) : \sigma_1 \geq A, \sigma_2 \geq B, \\
& \times \left(\sigma_1 - M - \frac{1-\theta}{1+\theta}D\right)\left(\sigma_2 - M + \frac{1-\theta}{1+\theta}D\right) \leq \frac{4\theta}{(1+\theta)^2}D^2 \Bigg\}, \\
\Theta_\theta^{--}(A, B) = \Bigg\{ & (\sigma_1, \sigma_2) : \sigma_1 \leq A, \sigma_2 \leq B, \\
& \times \left(\sigma_1 - M - \frac{1-\theta}{1+\theta}D\right)\left(\sigma_2 - M + \frac{1-\theta}{1+\theta}D\right) \leq \frac{4\theta}{(1+\theta)^2}D^2 \Bigg\}, \\
\Theta_\theta^{+-}(A, B) = \Bigg\{ & (\sigma_1, \sigma_2) : \sigma_1 \geq A, \sigma_2 \leq B, \\
& \times \left(\sigma_1 - M - \frac{1+\theta}{1-\theta}D\right)\left(\sigma_2 - M + \frac{1+\theta}{1-\theta}D\right) \geq -\frac{4\theta}{(1-\theta)^2}D^2 \Bigg\}, \\
\Theta_\theta^{-+}(A, B) = \Bigg\{ & (\sigma_1, \sigma_2) : \sigma_1 \leq A, \sigma_2 \geq B, \\
& \times \left(\sigma_1 - M - \frac{1+\theta}{1-\theta}D\right)\left(\sigma_2 - M + \frac{1+\theta}{1-\theta}D\right) \geq -\frac{4\theta}{(1-\theta)^2}D^2 \Bigg\}.
\end{aligned}$$

Finally, $\Theta_{1,\theta}(A, B)$ contains the box $\Theta_\theta^B(A, B)$ with sides parallel to $\sigma_2 = \sigma_1$ and $\sigma_2 = -\sigma_1$ and containing the points

$$\begin{aligned}
E &= \left(\frac{1+\sqrt{\theta}}{1-\sqrt{\theta}}D + M, -\frac{1+\sqrt{\theta}}{1-\sqrt{\theta}}D + M\right), \\
F &= \left(\frac{1-\sqrt{\theta}}{1+\sqrt{\theta}}D + M, -\frac{1-\sqrt{\theta}}{1+\sqrt{\theta}}D + M\right), \\
G &= \left(\frac{1+2\sqrt{\theta}-\theta}{1+\theta}D + M, \frac{-1+2\sqrt{\theta}+\theta}{1+\theta}D + M\right), \\
H &= \left(\frac{1-2\sqrt{\theta}-\theta}{1+\theta}D + M, \frac{-1-2\sqrt{\theta}+\theta}{1+\theta}D + M\right).
\end{aligned}$$

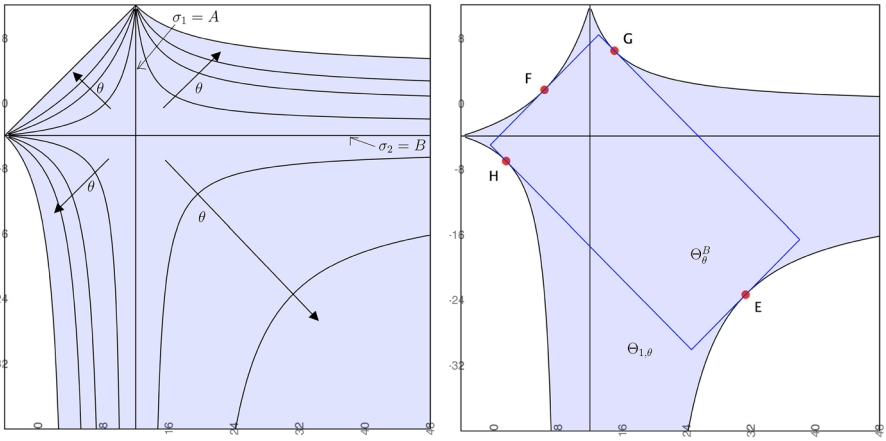

Fig. 4 *Left* level sets given by (16) for different values of θ; *right* set $\Theta_{1,\theta}$ given by (17) and box Θ_θ^B for the particular choice $\theta = 0.3$. $A = 12,\ B = -4$

Proof This is an elementary exercise and the proof is left to the reader.

In Fig. 4 we depicted the level sets (16) (left) and an example of regions $\Theta_{1,\theta}$ and Θ_θ^B (right).

4 Estimates of optimized interface parameters

In general, the optimal symbols $\sigma_1^{opt} = A(m, \boldsymbol{k})$ and $\sigma_2^{opt} = B(m, \boldsymbol{k})$ are not effective in the practice since they lead to non-local interface conditions which are hardly implementable. For this reason, it is a common practice to look for the best symbols within a specific subset, for example the constants (Optimized Schwarz Method, see, e.g, [15,17,18]). Given m and $\boldsymbol{k}$, we have in general that $A(m, \boldsymbol{k}) \neq -B(m, \boldsymbol{k})$, so that it does not make sense to look for the constant optimized value p such that the reduction factor computed for $\sigma_1 = p$ and $\sigma_2 = -p$ is minimized.

In order to simplify our study, we assume however that σ_1 and σ_2 are related. In other words, rather than looking for the best possible point (σ_1, σ_2) in $\mathbb{R}^2$, we will look for the best possible (σ_1, σ_2) belonging to a properly chosen curve

$$s(p) = \begin{cases} \widetilde{\sigma}_1(p) \\ \widetilde{\sigma}_2(p) \end{cases} \quad p \in \mathbb{R},$$

so that in fact we obtain a minimization problem over the single scalar parameter p. In particular, given the curve $s(p)$, we consider the following

Problem 1 *Find* $\widehat{p} \in \Gamma$ *which realizes*

$$\begin{aligned} \max_{(m,\boldsymbol{k})\in K} |\rho(m, \boldsymbol{k}, \widetilde{\sigma}_1(\widehat{p}), \widetilde{\sigma}_2(\widehat{p}))| &= \max_{(m,\boldsymbol{k})\in K} \left| \frac{\widetilde{\sigma}_1(\widehat{p}) - A(m, \boldsymbol{k})}{\widetilde{\sigma}_2(\widehat{p}) - A(m, \boldsymbol{k})} \cdot \frac{\widetilde{\sigma}_2(\widehat{p}) - B(m, \boldsymbol{k})}{\widetilde{\sigma}_1(\widehat{p}) - B(m, \boldsymbol{k})} \right| \\ &= \min_p \max_{(m,\boldsymbol{k})\in K} \left| \frac{\widetilde{\sigma}_1(p) - A(m, \boldsymbol{k})}{\widetilde{\sigma}_2(p) - A(m, \boldsymbol{k})} \cdot \frac{\widetilde{\sigma}_2(p) - B(m, \boldsymbol{k})}{\widetilde{\sigma}_1(p) - B(m, \boldsymbol{k})} \right|, \end{aligned}$$

where K is the set of the frequencies and $\Gamma \subset \mathbb{R}$ is the set where $s(p)$ is defined.

The problem now is to choose an appropriate curve $s(p)$. Assume (as it will be the case in our cases) that

$$\overline{B} := \max_{(m,\boldsymbol{k})\in K} B(m,\boldsymbol{k}) \leq \overline{A} := \min_{(m,\boldsymbol{k})\in K} A(m,\boldsymbol{k}). \tag{18}$$

Then, thanks to the definition of the set Θ_1 in (14), we have that the stripe $\mathcal{S}(\overline{A},\overline{B}) = \{(\sigma_1,\sigma_2) : \sigma_1 > \sigma_2$, and $2\overline{B} < \sigma_1 + \sigma_2 < 2\overline{A}\}$ is contained in $\Theta_1(A(m,\boldsymbol{k}), B(m,\boldsymbol{k}))$ for all $(m,\boldsymbol{k}) \in K$, so that for all points (σ_1,σ_2) in $\mathcal{S}(\overline{A},\overline{B})$ we have, owing to Theorem 1,

$$\left|\frac{\sigma_1-\overline{A}}{\sigma_2-\overline{A}}\cdot\frac{\sigma_2-\overline{B}}{\sigma_1-\overline{B}}\right| < 1.$$

We decided to look for the curve $s(p)$ within $\mathcal{S}(\overline{A},\overline{B})$, thus guaranteeing $|\rho| < 1$ for all $(m,\boldsymbol{k}) \in K$. The idea is to consider a curve which is far enough from the boundary of $\mathcal{S}(\overline{A},\overline{B})$. This guarantees that $s(p)$ is far from all the boundaries $\partial\Theta_1(A(m,\boldsymbol{k}), B(m,\boldsymbol{k}))$, where $|\rho| = 1$ for some $(m,\boldsymbol{k})$. To this aim, call

$$\overline{M} = \frac{1}{2}(\overline{A}+\overline{B}) \tag{19}$$

and consider the line s

$$\sigma_2 = -\sigma_1 + 2\overline{M}, \quad \sigma_1 \geq \overline{M}, \tag{20}$$

which divides in two equal parts $\mathcal{S}(\overline{A},\overline{B})$ and then is far from its boundary, see Fig. 5.

Then, as long as the points belonging to s are far from the line $\sigma_1 = \sigma_2$ and from infinity, they are far from the boundary of the set $\Theta_1(A(m,\boldsymbol{k}), B(m,\boldsymbol{k}))$ for whatever $(m,\boldsymbol{k}) \in K$, and therefore give $|\rho| < 1$ for whatever $(m,\boldsymbol{k}) \in K$. We look then for the best value of p such that the reduction factor is minimized by taking $\sigma_1 = p$, $\sigma_2 = -p + 2\overline{M}$. This justifies the study of the following

Problem 2 *Minimize the function*

$$p \mapsto \max_{(m,\boldsymbol{k})\in K} |\widehat{\rho}(p,m,\boldsymbol{k})| := \max_{(m,\boldsymbol{k})\in K} \left|\frac{p-A(m,\boldsymbol{k})}{-p+2\overline{M}-A(m,\boldsymbol{k})}\,\frac{-p+2\overline{M}-B(m,\boldsymbol{k})}{p-B(m,\boldsymbol{k})}\right|$$

for $p \geq \overline{M}$.

This optimization problem requires that we know exactly the functions $A(m,\boldsymbol{k})$ and $B(m,\boldsymbol{k})$. Nevertheless, one can obtain an interesting quantitative result even in the general case. Indeed, the following result holds.

Theorem 2 *Assume that $A(m,\boldsymbol{k})$ and $B(m,\boldsymbol{k})$ are bounded on some set K, with $B < A$ for all $(m,\boldsymbol{k}) \in K$, and call*

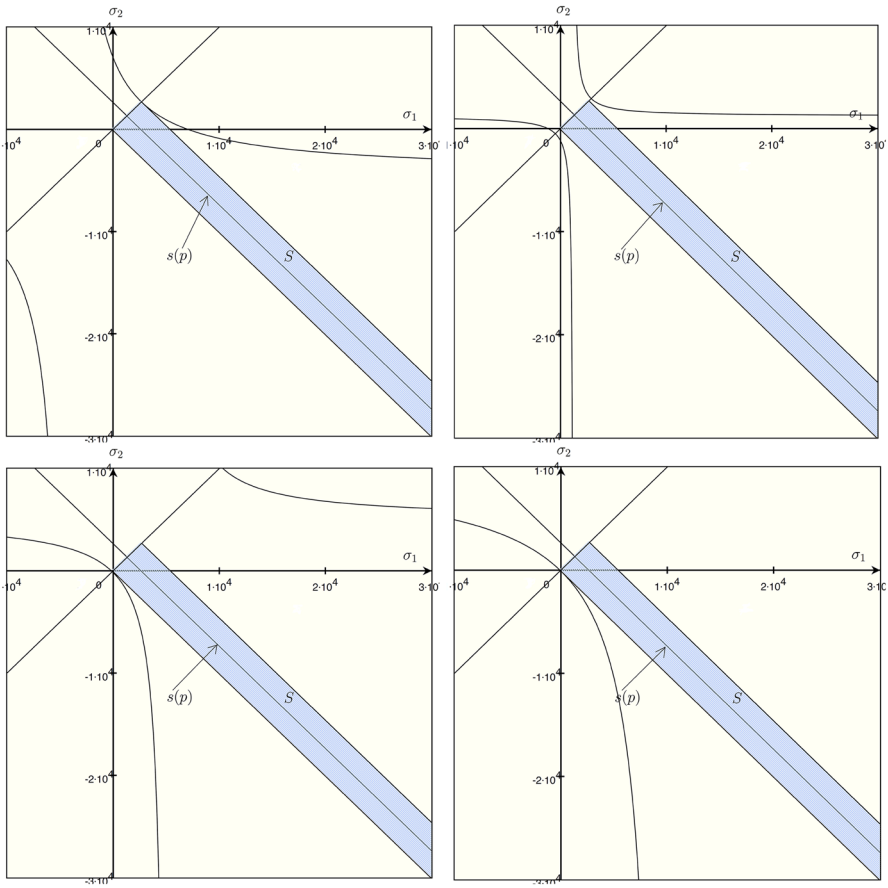

Fig. 5 Four possible scenarios with the stripe S for the particular choices $m = 0, k = 0.6$ (*top, left*); $m = 1, k = 0.6$ (*top, right*); $m = 0, k = 12.5$ (*bottom, left*); $m = 10, k = 12.5$ (*bottom, right*). FSI problem, A and B given by (45)–(48)

$$D(m,\boldsymbol{k}) = \frac{1}{2}(A(m,\boldsymbol{k}) - B(m,\boldsymbol{k})), \qquad M(m,\boldsymbol{k}) = \frac{1}{2}(A(m,\boldsymbol{k}) + B(m,\boldsymbol{k})), \quad (21)$$

$$Q(m,\boldsymbol{k}) = \frac{|M(m,\boldsymbol{k}) - \overline{M}|}{D(m,\boldsymbol{k})}, \ \overline{Q} = \sup_{(m,\boldsymbol{k})\in K} Q(m,\boldsymbol{k}), \ N = \frac{\inf_{(m,\boldsymbol{k})\in K} D(m,\boldsymbol{k})}{\sup_{(m,\boldsymbol{k})\in K} D(m,\boldsymbol{k})}, \quad (22)$$

with $\overline{M}$ *given by* (19). *Assume that* $\overline{A}$ *and* $\overline{B}$ *defined by* (18) *are such that* $\overline{B} < \overline{A}$ *and let*

$$\rho_0 = \max\left\{\left(\frac{1-\sqrt{N}}{1+\sqrt{N}}\right)^2; \left(\frac{1-\sqrt{1-\overline{Q}^2}}{\overline{Q}}\right)^2\right\}. \quad (23)$$

Then, for all $(m, \boldsymbol{k}) \in K$*, we have*

$$\widehat{\rho}(p, m, \boldsymbol{k}) = \left| \frac{p - A(m, \boldsymbol{k})}{2\overline{M} - p - A(m, \boldsymbol{k})} \frac{2\overline{M} - p - B(m, \boldsymbol{k})}{p - B(m, \boldsymbol{k})} \right| \leq \rho_0, \tag{24}$$

if and only if $p \in [p_-, p_+]$ *with*

$$\begin{aligned} p_- &= \overline{M} + \sup_{(m,\boldsymbol{k})\in K} \left\{ \tfrac{1+\rho_0}{1-\rho_0} D(m, \boldsymbol{k}) \right. \\ &\qquad \left. - \sqrt{(\overline{M} - M(m, \boldsymbol{k}))^2 + \tfrac{4\rho_0}{(1-\rho_0)^2} (D(m, \boldsymbol{k}))^2} \right\}, \\ p_+ &= \overline{M} + \inf_{(m,\boldsymbol{k})\in K} \left\{ \tfrac{1+\rho_0}{1-\rho_0} D(m, \boldsymbol{k}) \right. \\ &\qquad \left. + \sqrt{(\overline{M} - M(m, \boldsymbol{k}))^2 + \tfrac{4\rho_0}{(1-\rho_0)^2} (D(m, \boldsymbol{k}))^2} \right\}. \end{aligned} \tag{25}$$

Proof The proof is divided in two steps. In the first one, we look for the minimum value of θ which guarantees that the boxes Θ_θ^B have a non-empty intersection as $(m, \boldsymbol{k})$ varies in K . This value will be precisely ρ_0 defined in (23), and the intersection will be a box which crosses the line s in a segment. This means that all the points in this segment give $\widehat{\rho} \leq \rho_0$. Then, in the second part of the proof, we extend the endpoints of the box $\Theta_{\rho_0}^B$ lying on s as long as it is still guaranteed that $\widehat{\rho} \leq \rho_0$.

By hypothesis, $D(m, \boldsymbol{k}) \geq (\overline{A} - \overline{B})/2 > 0$, and this implies that $Q(m, \boldsymbol{k})$ is well defined and non negative. On the other hand,

$$\begin{aligned} 2|M(m, \boldsymbol{k}) - \overline{M}| &= |A(m, \boldsymbol{k}) + B(m, \boldsymbol{k}) - \overline{A} - \overline{B}| \\ &= |A(m, \boldsymbol{k}) - \overline{A} - (\overline{B} - B(m, \boldsymbol{k}))| \\ &\leq A(m, \boldsymbol{k}) - \overline{A} + (\overline{B} - B(m, \boldsymbol{k})) \\ &= 2D(m, \boldsymbol{k}) - (\overline{A} - \overline{B}). \end{aligned}$$

This implies

$$\begin{aligned} Q(m, \boldsymbol{k}) &\leq \frac{D(m, \boldsymbol{k}) - (\overline{A} - \overline{B})/2}{D(m, \boldsymbol{k})} = 1 - \frac{1}{2} \frac{\left(\overline{A} - \overline{B}\right)}{D(m, \boldsymbol{k})} \\ &\leq 1 - \frac{1}{2} \frac{\left(\overline{A} - \overline{B}\right)}{\sup_{(m,\boldsymbol{k})\in K} D(m, \boldsymbol{k})} < 1. \end{aligned}$$

Next, take ρ_0 satisfying

$$\rho_0 \geq \left(\frac{1 - \sqrt{N}}{1 + \sqrt{N}} \right)^2. \tag{26}$$

This implies

$$\frac{1 - \sqrt{\rho_0}}{1 + \sqrt{\rho_0}} \leq \sqrt{N},$$

so that by the definition of N we have

$$\widehat{p}_- := \sup_{(m,\boldsymbol{k})\in K} D(m,\boldsymbol{k})\frac{1-\sqrt{\rho_0}}{1+\sqrt{\rho_0}} + \overline{M} \le \widehat{p}_+ := \inf_{(m,\boldsymbol{k})\in K} D(m,\boldsymbol{k})\frac{1+\sqrt{\rho_0}}{1-\sqrt{\rho_0}} + \overline{M}. \tag{27}$$

By noticing that $p_- \le \widehat{p}_-$ and $p_+ \ge \widehat{p}_+$, we have from the previous inequality that the interval of p defined by (25) is non empty. Now, we observe that for any $p \in [\widehat{p}_-, \widehat{p}_+]$, and for any $(m,\boldsymbol{k}) \in K$, the points $(p, 2\overline{M} - p)$ belong to the box $\Theta^B_{\rho_0}(A(m,\boldsymbol{k}), B(m,\boldsymbol{k}))$. This is more easily seen after a rotation of $\pi/4$ (and a dilation of $1/\sqrt{2}$), given by

$$\zeta \begin{bmatrix} x \\ y \end{bmatrix} = \frac{1}{2}\begin{bmatrix} x-y \\ x+y \end{bmatrix}.$$

Thus we have to show that for any $p \in [\widehat{p}_-, \widehat{p}_+]$ and for any $(m,\boldsymbol{k}) \in K$, the points $(p - \overline{M}, \overline{M})$ belong to the axes-parallel box $\zeta\Theta^B_{\rho_0}(A(m,\boldsymbol{k}), B(m,\boldsymbol{k}))$ with sides containing the points (see Lemma 1)

$$\zeta E = \left(\frac{1+\sqrt{\rho_0}}{1-\sqrt{\rho_0}}D, M\right), \qquad \zeta F = \left(\frac{1-\sqrt{\rho_0}}{1+\sqrt{\rho_0}}D, M\right),$$
$$\zeta G = \left(\frac{1-\rho_0}{1+\rho_0}D, \frac{2\sqrt{\rho_0}}{1+\rho_0}D + M\right), \zeta H = \left(\frac{1-\rho_0}{1+\rho_0}D, \frac{-2\sqrt{\rho_0}}{1+\rho_0}D + M\right),$$

or equivalently that

$$\frac{1-\sqrt{\rho_0}}{1+\sqrt{\rho_0}}D \le p - \overline{M} \le \frac{1+\sqrt{\rho_0}}{1-\sqrt{\rho_0}}D,$$

and

$$\frac{-2\sqrt{\rho_0}}{1+\rho_0}D + M \le \overline{M} \le \frac{2\sqrt{\rho_0}}{1+\rho_0}D + M.$$

The first condition follows immediately from the definition of $\widehat{p}_-$ and $\widehat{p}_+$, see (27), while the second reduces to

$$Q(m,\boldsymbol{k}) = \frac{\left|\overline{M} - M(m,\boldsymbol{k})\right|}{D(m,\boldsymbol{k})} \le \frac{2\sqrt{\rho_0}}{1+\rho_0}.$$

The latter inequality holds true if

$$\overline{Q} \le \frac{2\sqrt{\rho_0}}{1+\rho_0}$$

that is for

$$\sqrt{\rho_0} \ge \frac{1-\sqrt{1-\overline{Q}^2}}{\overline{Q}}.$$

The latter condition, together with (26), are satisfied under hypothesis (23) and this concludes the first part of the proof.

The condition $p \in [\widehat{p}_-, \widehat{p}_+]$ provides a sufficient condition for the satisfaction of (24). We want now to extend such a range so to obtain also a necessary condi-tion. To this aim, observing that the box $\Theta^B_{\rho_0}(A\ (m, \boldsymbol{k})\ , B\ (m, \boldsymbol{k}))$ is contained in $\Theta_{1,\rho_0}(A\ (m, \boldsymbol{k})\ , B\ (m, \boldsymbol{k}))$ (see Lemma 1), we are sure to satisfy (24) until the line s does not intersect the boundary of $\Theta_{1,\rho_0}\ (A\ (m, \boldsymbol{k})\ , B\ (m, \boldsymbol{k}))$, defined by the two branches of the hyperbola

$$\left(\sigma_1 - M - \frac{1+\rho_0}{1-\rho_0}D\right)\left(\sigma_2 - M + \frac{1+\rho_0}{1-\rho_0}D\right) = -\frac{4\rho_0}{(1-\rho_0)^2}D^2,$$

see Lemma 1. Thus, replacing $\sigma_2 = 2\overline{M} - \sigma_1$ in the above equation gives

$$\left(\sigma_1 - M - \frac{1+\rho_0}{1-\rho_0}D\right)\left(-\sigma_1 + 2\overline{M} - M + \frac{1+\rho_0}{1-\rho_0}D\right) = -\frac{4\rho_0}{(1-\rho_0)^2}D^2$$

$$\sigma_1^2 - 2\left(\overline{M} + \frac{1+\rho_0}{1-\rho_0}D\right)\sigma_1 + 2M\overline{M} - M^2 + 2\frac{1+\rho_0}{1-\rho_0}D\overline{M} + D^2 = 0,$$

with solutions

$$\sigma_1 = \overline{M} + \frac{1+\rho_0}{1-\rho_0}D\ (m, \boldsymbol{k}) \pm \sqrt{\left(\overline{M} - M\ (m, \boldsymbol{k})\right)^2 + \frac{4\rho_0}{(1-\rho_0)^2}\left(D\ (m, \boldsymbol{k})\right)^2}.$$

Since we want that the points $(\ p,\ 2\overline{M} - p) \in \Theta_{1,\rho_0}(A\ (m, \boldsymbol{k})\ , B\ (m, \boldsymbol{k}))$ for all $(m, \boldsymbol{k}) \in K$, then it is necessary and sufficient that $p \in [p_-, p_+]$ defined in (25). □

In Fig. 6 we reported four possible sets Θ_{1,ρ_0} for different values of $(m, \boldsymbol{k})$. In particular, this figure as well as Fig. 5 are related to the fluid-structure interaction problem described below, where A and B are given by (45)–(48), and the other parameters are defined in Sect. 6.2. We notice that the points $s(\ p_-)$ and $s(\ p_+)$ are always in such sets.

Remark 2 One could obtain a sharper result in the previous Theorem by replacing $\overline{M} = \frac{1}{2}\left(A + \overline{B}\right)$ with the number that minimizes the quantity

$$\sup_{(m,\boldsymbol{k})\in K} \frac{\left|M\ (m, \boldsymbol{k}) - \overline{M}\right|}{D\ (m, \boldsymbol{k})}.$$

Of course such a choice can only be done if the functions $M\ (m, \boldsymbol{k})$ and $D\ (m, \boldsymbol{k})$ are known.

5 Examples of possible applications

In this section we present three possible applications of the general results reported above. In particular in Sects. 5.1 and 5.2 we present two problems considered so

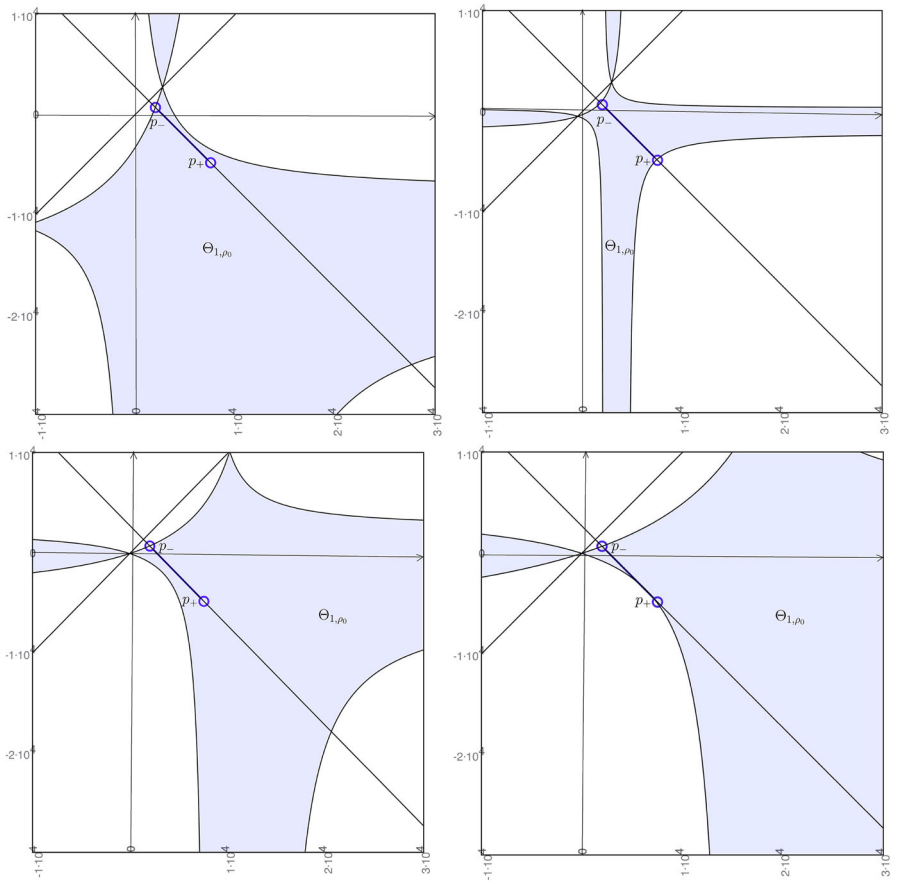

Fig. 6 Four possible sets $\Theta_{1,\rho_0}(\rho_0 = 0.32)$ for the particular choices $m = 0$, $k = 0.6$ (*top*, *left*); $m = 1$, $k = 0.6$ (*top*, *right*); $m = 0$, $k = 12.5$ (*bottom*, *left*); $m = 10$, $k = 12.5$ (*bottom*, *right*). FSI problem, A and B given by (45)–(48)

far in the literature, whereas in Sect. 5.3 we derive a completely new analysis and optimization for the fluid–structure interaction (FSI) problem.

5.1 The diffusion-reaction problem with a flat interface

This problem has been considered and analyzed in [15]. In particular, we have $n = 2$, $d = 1$, $a = -\infty$, $b = +\infty$, $R = 0$, and problem (8) with $\mathcal{L}_1 = \mathcal{L}_2 = -\triangle + \quad \xi$, $\xi > 0$, $\Omega \quad = \mathbb{R}^2$, $\Omega_1 = \{(x, y) \in \mathbb{R}^2 : x < 0, y \in \mathbb{R}\}$, $\Omega_2 = \{(x, y) \in \mathbb{R}^2 : x > 0, y \in \mathbb{R}\}$, $\Sigma \quad := \Sigma_0 = \{(x, y) \in \mathbb{R}^2 : x = 0, y \in \mathbb{R}\}$, $\gamma_1 = \gamma_2 = +\infty$ and $\delta = 1$. The only frequency coordinate is k, that is the one related to the longitudinal direction y. In this case, the solutions (10) are given by

$$\widehat{u_1}^j(x, k) = X_1^j(k) e^{x\sqrt{k^2+\xi}}, \quad \widehat{u_2}^j(x, k) = X_2^j(k) e^{-x\sqrt{k^2+\xi}},$$

for some functions X_1^j and X_2^j [15]. Then, the expressions in (11) become

$$A(k) = -B(k) = \sqrt{k^2 + \xi},$$

and the reduction factor (12) reads

$$\rho(k) = \frac{\sigma_1(k) - \sqrt{k^2+\xi}}{\sigma_2(k) - \sqrt{k^2+\xi}} \cdot \frac{\sigma_2(k) + \sqrt{k^2+\xi}}{\sigma_1(k) + \sqrt{k^2+\xi}}, \tag{28}$$

see also [15].

Now, by noticing that $A > B$ for all k, we can can apply Theorem 1, and we have from (14) that the exact convergence set is given by $\Theta = \Theta_1 \cup \Theta_2$, where

$$\Theta_1 = \{(\sigma_1, \sigma_2) : \sigma_2 < \sigma_1 \text{ and } \sigma_1\sigma_2 < k^2 + \xi\},$$
$$\Theta_2 = \{(\sigma_1, \sigma_2) : \sigma_2 > \sigma_1 \text{ and } \sigma_1\sigma_2 > k^2 + \xi\}.$$

Regarding the optimization procedure, we have from (19) that $\overline{M} = 0$, so that in this case it makes sense to look for the same optimal value, see also [15]. In particular, assuming $k \in [k_{min}, k_{max}]$, Problem 2 becomes

Problem 3 *Minimize the function*

$$p \mapsto \max_{k\in[k_{min},k_{max}]} \left| \frac{p - \sqrt{k^2+\xi}}{p + \sqrt{k^2+\xi}} \right|^2,$$

for $p \geq 0$.

From (21) and (22) we have $D(k) = \sqrt{k^2+\xi}$, $M(k) = Q(k) = \overline{Q} = 0$ and $N = \sqrt{\frac{k_{min}^2+\xi}{k_{max}^2+\xi}}$. Then, by noticing that $\lim_{x\to 0} \frac{1-\sqrt{1-x^2}}{x} = 0$, we have from (23)

$$\rho_0 = \left(\frac{1 - \sqrt[4]{\frac{k_{min}^2+\xi}{k_{max}^2+\xi}}}{1 + \sqrt[4]{\frac{k_{min}^2+\xi}{k_{max}^2+\xi}}} \right)^2.$$

Then, since the hypotheses of Theorem 2 hold true, by its application we have

$$|\widehat{\rho}| = \left| \frac{p - \sqrt{k^2+\xi}}{p + \sqrt{k^2+\xi}} \right|^2 \leq \left(\frac{1 - \sqrt[4]{\frac{k_{min}^2+\xi}{k_{max}^2+\xi}}}{1 + \sqrt[4]{\frac{k_{min}^2+\xi}{k_{max}^2+\xi}}} \right)^2$$

for all $k \in [k_{min}, k_{max}]$, provided that p belongs to the range defined by (25). Moreover, we have the following characterization of such a range:

$$\sqrt{k_{min}^2 + \xi} \leq p \leq \sqrt{k_{max}^2 + \xi}. \tag{29}$$

We observe that Problem 3 has been exhaustively studied in [15]. In particular, the following optimized value has been found:

$$p_{opt} = ((k_{min}^2 + \xi)(k_{max}^2 + \xi))^{1/4}, \tag{30}$$

leading to the best reduction factor $\rho_{opt} = \rho(k_{min}) = \rho(k_{max})$. We observe that the above value of p_{opt} falls in (29).

Just to provide a quantitative result, referring to the numerical simulations reported in [15, Table 6.3], we consider the diffusion-reaction problem solved in the unit square with $\xi = 100$ and $h = 1/50$. We then have $k_{min} = \pi/H = \pi$, with H the dimension of the domain, and $k_{max} = \pi/\ h = 50\pi$, with h the space discretization parameter. Then our estimates, using the range defined by (29), tell us that the reduction factor satisfies

$$|\widehat{\rho}| = \left| \frac{p - \sqrt{k^2 + \xi}}{p + \sqrt{k^2 + \xi}} \right|^2 \leq 0.35 \tag{31}$$

for all $k \in [\pi, 50\pi]$, provided that

$$10.5 \leq p \leq 157.4.$$

Moreover, from (30) we have $p_{opt} = 40.6$ with $\rho_{opt} = 0.35$. This highlights the optimality of estimate (31).

Remark 3 Observe that Eq. (3) does not depend on n but only on d. This means that the same analysis and optimization of above is obtained by considering the diffusion-reaction problem with a flat interface in 3D. Accordingly, in [18] the convergence factor (28) has been obtained also in the 3D case, provided that k is substituted by (k_1, k_2) with k_1 and k_2 the frequency coordinates related to the variables y_1 and y_2.

5.2 The diffusion-reaction problem with a cylindrical interface

This problem has been introduced and studied in [18] to consider those situations where the interface is not flat but of cylindrical type, see Fig. 2, right. In particular, we have $n = 3$, $d = 2$, $a = 0$, $b = +\infty$, and problem (8) with $\mathcal{L}_1 = \mathcal{L}_2 = -\triangle + \xi$, $\Omega = \mathbb{R}^3$, $\Omega_1 := \{(x_1, x_2, y) \in \mathbb{R}^3 : x_1^2 + x_2^2 < R^2\}$, $\Omega_2 := \{(x_1, x_2, y) \in \mathbb{R}^3 : x_1^2 + x_2^2 > R^2\}$, $\Sigma_R = \{(x_1, x_2, y) \in \mathbb{R}^3 : x_1^2 + x_2^2 = R^2\}$, $\gamma_2 = +\infty$, $\delta = 1$, and condition (7) holds. The frequency coordinates are $k \in \mathbb{R}$, related to the longitudinal direction y, and $m \in \mathbb{Z}$, related to the one-dimensional torus $S^1 = \{x_1^2 + x_2^2 = 1\}$. In this case, the solutions (10) are given by

$$\widehat{u_1}^j(r, m, k) = X_1^j(k) I_m(\alpha r), \quad \widehat{u_2}^j(r, m, k) = X_2^j(k) K_m(\alpha r),$$

for some functions $X1^j$ and $X2^j$, where $\alpha = \sqrt{k^2 + \xi}$, I_m and K_m are the modified Bessel functions, see [23], and $r = \sqrt{x_1^2 + x_2^2}$, as usual. Then, the expressions in (11) become

$$A(m,k) = -\alpha \frac{K'_m(\alpha R)}{K_m(\alpha R)}, \qquad B(m,k) = -\alpha \frac{I'_m(\alpha R)}{I_m(\alpha R)}, \tag{32}$$

see also [18]. Notice that owing to the properties of the modified Bessel functions, we have $A(m, k) > 0$, $\forall k, m$, and $B(m, k) < 0$, $\forall k, m$. Then, the reduction factor (12) reads

$$\rho(m,k) = \left| \frac{\sigma_1(m,k) + \alpha \frac{K'_m(\alpha R)}{K_m(\alpha R)}}{\sigma_2(m,k) + \alpha \frac{K'_m(\alpha R)}{K_m(\alpha R)}} \cdot \frac{\sigma_2(m,k) + \alpha \frac{I'_m(\alpha R)}{I_m(\alpha R)}}{\sigma_1(m,k) + \alpha \frac{I'_m(\alpha R)}{I_m(\alpha R)}} \right|,$$

see also [18].

Now, we can apply again Theorem 1, and we have from (14) that the exact conver-gence set is given by $\Theta = \Theta_1 \cup \Theta_2$, where

$$\begin{aligned}
\Theta_1 = \Bigg\{ & (\sigma_1, \sigma_2) : \sigma_2 < \sigma_1 \text{ and } \left(\sigma_1 + \frac{\alpha}{2}\left(\frac{K'_m(\alpha R)}{K_m(\alpha R)} + \frac{I'_m(\alpha R)}{I_m(\alpha R)}\right)\right) \\
& \times \left(\sigma_2 + \frac{\alpha}{2}\left(\frac{K'_m(\alpha R)}{K_m(\alpha R)} + \frac{I'_m(\alpha R)}{I_m(\alpha R)}\right)\right) < \left(\frac{\alpha}{2}\left(\frac{K'_m(\alpha R)}{K_m(\alpha R)} - \frac{I'_m(\alpha R)}{I_m(\alpha R)}\right)\right)^2 \Bigg\}, \\
\Theta_2 = \Bigg\{ & (\sigma_1, \sigma_2) : \sigma_2 > \sigma_1 \text{ and } \left(\sigma_1 + \frac{\alpha}{2}\left(\frac{K'_m(\alpha R)}{K_m(\alpha R)} + \frac{I'_m(\alpha R)}{I_m(\alpha R)}\right)\right) \\
& \times \left(\sigma_2 + \frac{\alpha}{2}\left(\frac{K'_m(\alpha R)}{K_m(\alpha R)} + \frac{I'_m(\alpha R)}{I_m(\alpha R)}\right)\right) > \left(\frac{\alpha}{2}\left(\frac{K'_m(\alpha R)}{K_m(\alpha R)} - \frac{I'_m(\alpha R)}{I_m(\alpha R)}\right)\right)^2 \Bigg\}.
\end{aligned}$$

Regarding the optimization procedure, first of all we notice that the function A is increasing both in k and in m, whereas B is decreasing both in k and in m, see [18]. Then, assuming $k \in [k_{min}, k_{max}]$ and $m \in [m_{min}, m_{max}]$, from (18) we have $\overline{A} = -\alpha_{min} \frac{K'_{m_{min}}(\alpha_{min} R)}{K_{m_{min}}(\alpha_{min} R)}$ and $\overline{B} = -\alpha_{min} \frac{I'_{m_{min}}(\alpha_{min} R)}{I_{m_{min}}(\alpha_{min} R)}$, where we have set $\alpha_{min} = \sqrt{k_{min}^2 + \xi}$. Then, (19) gives

$$\overline{M} = -\frac{\alpha_{min}}{2}\left(\frac{K'_{m_{min}}(\alpha_{min} R)}{K_{m_{min}}(\alpha_{min} R)} + \frac{I'_{m_{min}}(\alpha_{min} R)}{I_{m_{min}}(\alpha_{min} R)}\right), \tag{33}$$

so that Problem 2 becomes

Problem 4 *Minimize the function*

$$p \mapsto \max_{\substack{m \in [m_{min}, m_{max}] \\ k \in [k_{min}, k_{max}]}} \left| \frac{p + \alpha \frac{K'_m(\alpha R)}{K_m(\alpha R)}}{-p + 2\overline{M} + \alpha \frac{K'_m(\alpha R)}{K_m(\alpha R)}} \frac{-p + 2\overline{M} + \alpha \frac{I'_m(\alpha R)}{I_m(\alpha R)}}{p + \alpha \frac{I'_m(\alpha R)}{I_m(\alpha R)}} \right|,$$

for $p \geq \overline{M}$ and with $\overline{M}$ given by (33).

We can then compute numerically from (22) the values of $\overline{Q}$ and N and apply again Theorem 2 obtaining a quantitative convergence result.

We observe that Problem 4 has been studied in [18] under the assumption $\overline{M} = 0$. Indeed, it has been there noticed that $A \simeq -B$ for general frequencies, apart for small values of m, k and ξ at the same time. In particular, the following optimized value has been found:

$$p_{opt} = \sqrt{-\frac{A_+ B_+ (A_- - B_-) + A_- B_- (A_+ - B_+)}{A_+ - B_+ - A_- + B_-}}, \tag{34}$$

where $A_- := A(m_{min}, k_{min})$, $B_- := B(m_{min}, k_{min})$, $A_+ := A(m_{max}, k_{max})$, $B_+ := B(m_{max}, k_{max})$, and A, B given by (32).

Referring to the numerical results shown in [18], we report here again a quantitative example to illustrate the application of our results. Take a cylinder whose length is 5 cm and radius 1 cm and where the interface is located at $R = 0.5$. For $\xi = 1$, $k_{min} = 0$, $k_{max} = 62$, $m_{min} = 0$, $m_{max} = 20$, we obtain $\overline{A} = 1.79$, $\overline{B} = -0.24$, $\overline{M} = 0.77$ so that our estimate based on (27) gives that

$$|\widehat{\rho}| = \left| \frac{p + \alpha \frac{K_m'(\alpha R)}{K_m(\alpha R)}}{-p + 1.54 + \alpha \frac{K_m'(\alpha R)}{K_m(\alpha R)}} \frac{-p + 1.54 + \alpha \frac{I_m'(\alpha R)}{I_m(\alpha R)}}{p + \alpha \frac{I_m'(\alpha R)}{I_m(\alpha R)}} \right| \leq 0.62$$

for all $k \in [0, 62]$ and $m \in [0, 20]$, provided that

$$9.437 \leq p \leq 9.439.$$

Moreover, from (34) we have $p_{opt} = 8.70$ with $\rho_{opt} = 0.62$. Observe that in this case p_{opt} does not fall in the range estimated by our result. This is not surprising, since the two optimization procedures have been performed with different values of $\overline{M}$. However, we observe that ρ_{opt} is precisely equal to ρ_0.

5.3 The fluid–structure interaction problem with a cylindrical interface

5.3.1 Problem setting

We are in the case of a cylindrical interface, that is $n = 3$, $d = 2$. We consider the problem arising from the interaction between an incompressible, inviscid and linear fluid occupying the domain $\Omega_f := \{(x_1, x_2, y) \in \mathbb{R}^3 : x_1^2 + x_2^2 < R^2\}$, and a linear elastic structure modeled with the wave equation occupying the domain $\Omega_s := \{(x_1, x_2, y) \in \mathbb{R}^3 : R^2 < x_1^2 + x_2^2 < (R+H)^2\}$. The two subproblems interact at the common interface $\Sigma_R = \{(x_1, x_2, y) \in \mathbb{R}^3 : x_1^2 + x_2^2 = R^2\}$. In particular, after a time discretization (for the sake of simplicity we consider here a BDF1 scheme for both subproblems, see [19]), the coupled problem at time $t^{n+1} := (n+1)\Delta t$, Δt being the time discretization parameter, reads

$$
\begin{cases}
\rho_f \delta_t \boldsymbol{u} + \nabla p = \boldsymbol{0} & \text{in } \Omega_f, \\
\nabla \cdot \boldsymbol{u} = 0 & \text{in } \Omega_f, \\
\int_{-\infty}^{\infty} \int_{S^1} |p(r\boldsymbol{x}', \boldsymbol{y})| d\sigma(\boldsymbol{x}') d\boldsymbol{y} & \text{bounded as } r \to 0^+, \\
\boldsymbol{u} \cdot \boldsymbol{n} = \delta_t \boldsymbol{\eta} \cdot \boldsymbol{n} & \text{on } \Sigma_R, \\
-p\boldsymbol{n} = \lambda \nabla \boldsymbol{\eta}\, \boldsymbol{n} & \text{on } \Sigma_R, \\
\boldsymbol{\eta} \times \boldsymbol{n} = \boldsymbol{0} & \text{on } \Sigma_R \\
\rho_s \delta_{tt} \boldsymbol{\eta} - \lambda \triangle \boldsymbol{\eta} = \boldsymbol{0} & \text{in } \Omega_s, \\
\gamma_{ST} \boldsymbol{\eta} + \lambda \nabla \boldsymbol{\eta}\, \boldsymbol{n} = P_{ext}\, \boldsymbol{n} & \text{on } \Sigma_{out},
\end{cases}
\tag{35}
$$

where, as usual, $r = \sqrt{x_1^2 + x_2^2}$, ρ_f and ρ_s are the fluid and structure densities, λ the square of the wave propagation velocity, $\delta_t w := \frac{w - w^n}{\Delta t}$, $\delta_{tt} w := \frac{\delta_t w - \delta_t w^n}{\Delta t}$, $\Sigma_{out} = \Sigma_{R+H} = \{(x_1, x_2, y) \in \mathbb{R}^3 : x_1^2 + x_2^2 = (R + H)^2\}$ is the external surface of the structure domain, $\boldsymbol{n}$ is the unit vector orthogonal to the interface Σ_R or Σ_{R+H} defined by $\boldsymbol{n} = \frac{(x_1, x_2, 0)}{\sqrt{x_1^2 + x_2^2}}$, and we have omitted the time index $n + 1$. Problem $(35)_{1-3}$ is the fluid problem, problem $(35)_{7-8}$ is the structure problem equipped with a Robin condition at the external surface to account for the effect of an elastic surrounding tissue with elasticity modulus γ_{ST} [27], P_{ext} is the external pressure, whereas $(35)_{4-6}$ are the coupling conditions at the FS interface. The fluid and the structure problems have to be completed with initial and boundary conditions along the y direction, the latter reducing to the assumption of decay to zero for $|y| \to \infty$. We also observe that the coupling at the interface is allowed only in the normal direction.

By combining linearly $(35)_4$ and $(35)_5$ we obtain two generalized Robin boundary conditions. Observe that in the fluid problem the viscous terms have been neglected so that the fluid Cauchy stress tensor reduces to the only pressure. In particular, setting $u_r = \boldsymbol{u} \cdot \boldsymbol{n}$ and $\eta_r = \boldsymbol{\eta} \cdot \boldsymbol{n}$ and introducing the operator $\mathcal{S}_f$, we obtain

$$
\mathcal{S}_f u_r - p = \mathcal{S}_f \delta_t \eta_r + \lambda\, \partial_r \eta_r\,,
$$

that is

$$
\mathcal{S}_f \Delta t\, \delta_t u_r - p = \mathcal{S}_f \delta_t \eta_r + \lambda\, \partial_r \eta_r - S_f u_r^n.
$$

Then, the transmission condition for the fluid problem can be rearranged as

$$
\mathcal{S}_f \Delta t\, \delta_t u_r - p = \frac{\mathcal{S}_f}{\Delta t}\, \eta_r + \lambda\, \partial_r \eta_r + F_1(u_r^n, \eta_r^n),
\tag{36}
$$

where F_1 accounts for terms at previous time steps. Analogously, by introducing the operator $\mathcal{S}_s$, we obtain the following interface condition for the structure problem

$$
\frac{\mathcal{S}_s}{\Delta t}\, \eta_r + \lambda\, \partial_r \eta_r = \mathcal{S}_s \Delta t\, \delta_t u_r - p + F_2(u_r^n, \eta_r^n),
\tag{37}
$$

where again F_2 accounts for terms at previous time steps. Then, at time t^{n+1}, the corresponding iterative generalized Schwarz method reads:

Given $\boldsymbol{u}^0$, p^0, η^0, solve for $j \geq 0$ until convergence

1. Fluid problem

$$\begin{cases} \rho_f \delta_t \boldsymbol{u}^{j+1} + \nabla p^{j+1} = \boldsymbol{0} & \text{in } \Omega_f, \\ \nabla \cdot \boldsymbol{u}^{j+1} = 0 & \text{in } \Omega_f, \\ \int_{-\infty}^{\infty} \int_{S^1} |p(r\boldsymbol{x}', \boldsymbol{y})| d\sigma(\boldsymbol{x}') d\boldsymbol{y} & \text{bounded as } r \to 0^+, \\ \mathcal{S}_f \Delta t \, \delta_t u_r^{j+1} - p^{j+1} = \dfrac{\mathcal{S}_f}{\Delta t} \eta_r^j + \lambda \, \partial_r \eta_r^j + F_1(u_r^n, \eta_r^n) & \text{on } \Sigma_R; \end{cases} \tag{38}$$

2. Structure problem

$$\begin{cases} \rho_s \delta_{tt} \boldsymbol{\eta}^{j+1} - \lambda \, \triangle \boldsymbol{\eta}^{j+1} = \boldsymbol{0} & \text{in } \Omega_s, \\ \gamma_{ST} \boldsymbol{\eta}^{j+1} + \lambda \nabla \boldsymbol{\eta}^{j+1} \boldsymbol{n} = P_{ext} \boldsymbol{n} & \text{on } \Sigma_{out}, \\ \dfrac{\mathcal{S}_s}{\Delta t} \eta_r^{j+1} + \lambda \, \partial_r \eta_r^{j+1} = \mathcal{S}_s \Delta t \, \delta_t u_r^{j+1} - p^{j+1} + F_2(u_r^n, \eta_r^n) & \text{on } \Sigma_R, \\ \boldsymbol{\eta}^{j+1} \times \boldsymbol{n} = \boldsymbol{0} & \text{on } \Sigma_R \end{cases} \tag{39}$$

5.3.2 Convergence analysis

In order to perform a convergence analysis of the generalized Schwarz method (38)–(39), we need to write the coupled problem (35) in a different manner, such that it falls in the general framework of problem (8). To this aim, we first notice that the divergence free condition on $\boldsymbol{u}$ $(35)_2$ allows us to rewrite the fluid problem $(35)_{1-3}$ only in the unknown pressure

$$\begin{cases} \triangle p = 0 & \text{in } \Omega_f, \\ \displaystyle\int_{-\infty}^{\infty} \int_{S^1} |p(r\boldsymbol{x}', \boldsymbol{y})| d\sigma(\boldsymbol{x}') d\boldsymbol{y} & \text{bounded as } r \to 0^+. \end{cases} \tag{40}$$

Then, we notice that structure problem $(35)_{7-8}$ along the r direction reads as follows

$$\begin{cases} \left(\dfrac{\rho_s}{\Delta t^2} - \lambda \triangle \right) \eta_r = 0 \text{ in } \Omega_s, \\ \gamma_{ST} \eta_r + \lambda \partial_r \eta_r = 0 \quad \text{on } \Sigma_{out}, \end{cases} \tag{41}$$

where we have set to zero the forcing term P_{ext} and the quantities at the previous time steps, since we analyze the convergence to the zero solution.

Following [17], thanks to the relation

$$\frac{\partial p}{\partial r} = -\rho_f \delta_t u_r = -\frac{\rho_f}{\Delta t}(u_r - u_r^n) \quad \text{on } \Sigma_R, \tag{42}$$

obtained by restricting the first equation of the fluid problem $(35)_1$ on the FS interface, it is possible to rewrite the interface conditions $(35)_{4-5}$ along the normal direction in terms of the pressure solely as follows

$$\begin{aligned} p &= -\lambda \frac{\partial \eta_r}{\partial r} \qquad \text{on } \Sigma_R, \\ \frac{\partial p}{\partial r} &= -\frac{\rho_f}{\Delta t^2}\eta_r \quad \text{on } \Sigma_R, \end{aligned} \tag{43}$$

where we have set to zero the terms at time n since we analyze the convergence to the zero solution. The previous interface conditions are of type $(6)_{3,4}$ with $u_1 = p$, $u_2 = \eta_r$, $\delta = 0$, $\kappa_D = -1$, $\kappa_N = -\frac{\rho_f}{\Delta t^2}$. Then, the FSI problem written in terms of the fluid pressure and structure displacement given by (40), (41), (43) falls in the general framework of problem (6), where $\mathcal{L}_1 = -\triangle$, $\mathcal{L}_2 = -\lambda\triangle + \frac{\rho_s}{\Delta t^2}$, $\Omega_1 = \Omega_f$, $\Omega_2 = \Omega_s$, $\gamma_2 = \gamma_{ST}$ for $r = R + H$. Analogously, owing to (42), conditions (36) and (37) could be rewritten as follows

$$\begin{aligned} &\frac{\rho_f}{\Delta t}{\mathcal{S}_f}^{-1} p + \frac{\partial p}{\partial r} = -\frac{\rho_f}{\Delta t^2}\eta_r - \frac{\rho_f \lambda}{\Delta t}{\mathcal{S}_f}^{-1}\frac{\partial \eta_r}{\partial r} \quad \text{on } \Sigma_R, \\ &\frac{\rho_f}{\Delta t^2}\eta_r + \frac{\lambda\rho_f}{\Delta t}\mathcal{S}_s^{-1}\frac{\partial \eta_r}{\partial r} = -\frac{\rho_f}{\Delta t}\mathcal{S}_s^{-1} p - \frac{\partial p}{\partial r} \quad \text{on } \Sigma_R, \end{aligned} \tag{44}$$

where we have set $F_1 = F_2 = 0$ since we analyze the convergence to the zero solution. Then, it is easy to check that the FSI problem given by (40), (41) and (44) falls in the general framework of problem (8) where $\mathcal{S}_1 = \frac{\rho_f}{\Delta t}{\mathcal{S}_f}^{-1}$, $\mathcal{S}_2 = \frac{\rho_f}{\Delta t}{\mathcal{S}_s}^{-1}$.

We have the following

Proposition 2 *Set*

$$A(m,k) = -\frac{\lambda\Delta t\beta(K_m'(\beta\, R) - \chi\, I_m'(\beta\, R))}{K_m(\beta\, R) - \chi\, I_m(\beta\, R)}, \qquad B(m,k) = -\frac{\rho_f\, I_m(kR)}{\Delta t\, k\, I_m'(kR)}. \tag{45}$$

Then, the reduction factor of iterations (38)–(39) *is given by*

$$\rho^j(m,k) = \rho(m,k) = \left| \frac{\sigma_f(m,k) - A(m,\boldsymbol{k})}{\sigma_s(m,k) - A(m,\boldsymbol{k})} \cdot \frac{\sigma_s(m,k) - B(m,\boldsymbol{k})}{\sigma_f(m,k) - B(m,\boldsymbol{k})} \right|, \tag{46}$$

where σ_f and σ_s are the symbols of $\mathcal{S}_f$ and $\mathcal{S}_s$, respectively, and where we have set

$$\beta(k) := \sqrt{k^2 + \frac{\rho_s}{\lambda\Delta t^2}}, \tag{47}$$

and

$$\chi(m,k) := \frac{\gamma_{ST}\, K_m\,(\beta(R+H)) + \lambda\beta K_m'(\beta(R+H))}{\gamma_{ST}\, I_m(\beta(R+H)) + \lambda\beta I_m'(\beta(R+H))}. \tag{48}$$

Moreover, the exact convergence set is given by (14) *with $\sigma_1 = \sigma_f$, $\sigma_2 = \sigma_s$ and A and B given by* (45).

Proof We need to determine the solutions of problems (40) and (41) at iteration j. Regarding the fluid problem (40), from (4) with $d = 2$ we obtain $\widehat{p}^{\,j+1}(r,m,k) = X_{f,1}^{j+1}(m,k)\, I_m(kr) + X_{f,2}^{j+1}(m,k)\, K_m(kr)$, for suitable functions $X_{f,1}^{j}$ and $X_{f,2}^{j}$, where

the dependence on l vanished since for $d = 2$ the multiplicity of the eigenvalues related to the spherical harmonics is constant ($k_m = 2$). The boundedness assumption $(40)_2$ on the pressure together with the properties of the modified Bessel functions entail $X^{j+1}_{f,2}(m,k) = 0,\ \forall j$, thus

$$\widehat{p}^{\,j+1}(r,m,k) = X^{j+1}_{f}(m,k)\, I_m(kr),$$

where, for the sake of simplicity, we have set $X^{j+1}_{f,1}(m,k) = X^{j+1}_{f}(m,k)$.

Regarding the structure problem $(41)_1$, from (4) with $d = 2$ we obtain $\widehat{\eta}^{\,j}_r(r,m,k) = X^j_{s,1}(m,k)\, I_m(\beta r) + X^j_{s,2}(m,k)\, K_m(\beta r)$ for suitable functions $X^j_{s,1}$ and $X^j_{s,2}$ and with β given by (47). Now, we impose condition $(41)_2$, obtaining

$$\gamma_{ST}\widehat{\eta}^{\,j}_r + \lambda\partial_r\widehat{\eta}^{\,j}_r = 0 \qquad \text{on } \widehat{\Sigma}_{out} := \{r = R + H,\ m \in \mathbb{N},\ k \in \mathbb{R}\}.$$

This leads to

$$\gamma_{ST}(X^j_{s,1} I_m(\beta r) + X^j_{s,2} K_m(\beta r)) + \lambda\beta\ (X^j_{s,1} I'_m(\beta r) + X^j_{s,2} K'_m(\beta r))\Big|_{r=R+H} = 0,$$

and thus to $X^j_{s,1} = -\chi\ X^j_{s,2}$, where χ is given by (48). Therefore, the structure solution is

$$\widehat{\eta}^{\,j}_r(r,m,k) = X^j_s(m,k)\,[K_m(\beta r) - \chi(m,k) I_m(\beta r)]\,,$$

where, for the sake of simplicity, we have set $X^j_{s,2}(m,k) = X^j_s(m,k)$.

Now, the direct application of Proposition 1 with $g_1(m,k) = I_m(kr)$ and $g_2(m,k) = K_m(\beta r) - \chi(m,k) I_m(\beta r)$ leads to the first part of thesis.

The second part of the thesis is a straightforward application of Theorem 1. □

Remark 4 In the case $\sigma_f \to \infty$, $\sigma_s = 0$ we obtain the *Dirichlet–Neumann* scheme, which is known to be characterized by poor convergence properties when the fluid and structure densities are similar, as happens in haemodynamics (*added mass effect*, see [5,14]) This is confirmed by our analysis which leads for the Dirichlet–Neumann scheme to the following reduction factor:

$$\rho^{DN}(m,k) = \frac{\rho_f\, I_m(k\,R)\,(K_m(\beta\,R) - \chi\, I_m(\beta\,R))}{\lambda\Delta t\beta\,\left(K'_m(\beta\,R) - \chi\, I'_m(\beta\,R)\right)\Delta t\, k\, I'_m(k\,R)},$$

which increases for big values of the ratio $\rho_f/\beta = \rho_f/\sqrt{\rho_s/(\lambda\Delta t^2) + k^2}$, that is when the fluid and structure densities are similar.

5.3.3 Optimization

The optimal symbols which guarantee that the reduction factor (46) annihilates are $\sigma^{opt}_f(m,k) = A(m,k)$ and $\sigma^{opt}_s(m,k) = B(m,k)$, where A and B are given by (45). Again, these quantities lead to non-implementable interface conditions, so that we

apply the theory developed in Sect. 4, allowing to obtain an optimization problem with respect to a scalar variable solely. We observe that in this case the determination of the maximum and of the minimum of $A(m, k)$ in (45) is not trivial, so that it is not possible anymore to write an explicit expression for $\overline{M}$, which needs to be computed numerically, see the next section.

6 Numerical results

In this section we present some numerical results to highlight the effectiveness of the theoretical findings reported in the previous sections for the FSI problem.

6.1 Generalities

We considered the coupling between the incompressible Navier–Stokes equations written in the Arbitrary Lagrangian–Eulerian formulation [8] and the linear infinitesimal elasticity, see for example [28]. In particular, we studied the effectiveness of the estimates reported in Sect. 5.3 and obtained for the simplified models, when applied to complete fluid and structure models. To do this, we compared their performance with the one related to the optimized values of σ_f and σ_s reported in [17], where the linear/non-viscous fluid $(35)_{1-2}$ has been coupled with the independent rings model for a membrane [12,30], and where the 2D convergence analysis and optimization have been performed in the case of a flat interface. In particular, the following optimized values have been found

$$\sigma_f^{flat} = \left(\frac{\rho_s H_s}{\Delta t} + \varphi \Delta t \right), \qquad \sigma_s^{flat} = \frac{2\rho_f}{\Delta t \, k_{max}},$$

where $\varphi = \frac{E H_s}{(1-\nu^2)R^2}$, with H_s the structure thickness, E the Young modulus, ν the Poisson modulus, and R the fluid domain radius. As noticed in [13], when the surrounding tissue is considered, the membrane models need to be rewritten by incorporating the surrounding elasticity coefficient γ_{ST} in the membrane elastic coefficient, that is by substituting φ with $\varphi + \gamma_{ST}$. Then, the optimized values related to the 2D/flat analysis become

$$\sigma_f^{flat} = \left(\frac{\rho_s H_s}{\Delta t} + (\varphi + \gamma_{ST}) \, \Delta t \right), \qquad \sigma_s^{flat} = \frac{2\rho_f}{\Delta t \, k_{max}}. \tag{49}$$

In all the numerical experiments, we used the BDF scheme of order 1 for both the subproblems with a semi-implicit treatment of the fluid convective term. Moreover, we used the following data: fluid viscosity $\mu = 0.0035\,\mathrm{kg/(m\,s)}$, fluid density $\rho_f = 1{,}000\,\mathrm{kg/m^3}$, structure density $\rho_s = 1{,}100\,\mathrm{kg/m^3}$, Poisson ratio $\nu = 0.49$, Young modulus $E = 3 \times 10^5\,\mathrm{Pa}$. All these data are inspired from haemodynamic applications where the computational domains are often characterized by a cylindrical shape, see, e.g, [12]. We observe that the simplified structure model $(35)_7$ considered in the analysis is characterized by only two parameters, ρ_s and λ, whereas the linear infinitesimal elasticity considered in the numerical experiments by three parameters,

ρ_s and the Lamé constants $\lambda_1 = E/(2(1+\nu))$ and λ_2. Here, to compute $A(m,k)$ in (45) and the other quantities needed to build the estimates reported in Theorem 2, we assumed that the value of λ could be approximated by $G\lambda_1$, with $G = \pi^2/12$ the Timoshenko correction factor.

We prescribed in all the numerical experiments the following pressure P_{in} at the inlet

$$P_{in} = \begin{cases} 100\text{Pa} & t \leq 0.08\,\text{s}, \\ 0 & 0.08\,\text{s} < t \leq T, \end{cases}$$

where $T = 0.20\,\text{s}$, and absorbing resistance conditions at the outlets [28,30].

In all the cases the optimized interface symbols are constant so that the Optimized Schwarz Method coincides with the Robin–Robin algorithm, introduced in the FSI context in [2] and then also considered in [1,3,31]. The fluid domain has been treated explicitly (semi-implicit approach, see [4,10,28,29]).

For the numerical discretization, we used $P1bubble - P1$ finite elements for the fluid subproblem and $P1$ finite elements for the structure subproblem, and a time discretization parameter $\Delta t = 0.001\,\text{s}$

All the numerical results have been obtained with the parallel Finite Element library `LIFEV` [24] developed at MOX—Politecnico di Milano, INRIA—Paris, CMCS—EPF of Lausanne and Emory University—Atlanta.

6.2 The case of a straight cylinder

In the first set of numerical experiments, we considered a cylinder with length $L = 0.05\,\text{m}$, partitioned in two non-overlapping subdomains, an inner cylinder for the fluid problem with radius $R = 0.005\,\text{m}$, 4,680 tetrahedra and 1,050 vertices (corresponding to 7,830 degrees of freedom for the velocity and 1,050 for the pressure), and an external cylindrical crown for the structure with thickness H_s and 1,260 vertices (corresponding to 3,780 degrees of freedom for the structure displacement). We studied the performance of the Optimized Schwarz Method when the thickness structure is $H_s = 0.001\,\text{m}$ and $H_s = 0.005\,\text{m}$ and the surrounding tissue parameter is $\gamma_{ST} = 1.5 \times 10^7\,\text{Pa/m}$ and $\gamma_{ST} = 3 \times 10^7\,\text{Pa/m}$. The space discretization parameter along the axial direction is $h = 0.0025\,\text{m}$, and the frequencies vary in the ranges $m = 0, \ldots, 10$ and $60 \leq k \leq 1{,}250\,\text{m}^{-1}$.

In Table 1 we report the values of M and ρ_0 and the optimal ranges of p derived by the estimates provided by Theorem 2.

In all the cases, we ran the simulations with different values of p within the estimated ranges, in order to find the best one. In Fig. 7 we reported the fluid pressure in the deformed domain at four different instants.

In Table 2 we reported the average number of iterations per time step to reach convergence and the normalized CPU time for the values of p within the estimated ranges which guaranteed the best convergence properties, and for the values of σ_f and σ_s provided by (49). Moreover, we reported the average number of iterations per time step for the classical Dirichlet–Neumann (DN) scheme. It is well-known that

Table 1 Values of M, $\overline{\rho_0}$ and of the optimal range of p provided by the estimates in Theorem 2

H_s	γ_{ST}	$\overline{M}$	ρ_0	$p \in$
0.001	1.5×10^7	79,300	0.42	[112,300, 638,300]
0.001	3.0×10^7	132,300	0.32	[198,300, 752,100]
0.005	1.5×10^7	86,400	0.41	[126,000, 720,900]
0.005	3.0×10^7	100,800	0.38	[145,900, 735,400]

Cylindrical simulation

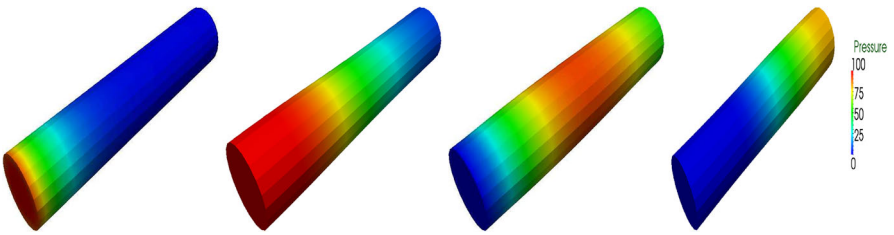

Fig. 7 Fluid pressure wave traveling along the deformed computational domain. From *left* to *right*, we have $t = 0.001$ s, $t = 0.004$ s, $t = 0.009$ s, $t = 0.013$ s

this scheme does not converge in general in the haemodynamic context without any relaxation, due to the added mass effect [5,6]. For this reason, we have considered an Aitken procedure to dynamically provide the value of the relaxation parameter [22]. Observe from this result the robustness of the optimized values estimated by Theorem 2. Indeed, the average number of iterations per time step seems to be independent of the parameters. On the contrary, the optimized interface parameters estimated with the 2D/flat analysis worked very well for small values of the structure thickness H_s (obtaining however worse performance with respect to the ones obtained by our analysis), whereas they did not work as well for a greater value of H_s. Accordingly, the CPU time increased in all the cases, especially for the case $H_s = 0.005$. This is reasonable since the 2D/flat analysis assumes a membrane model for the structure. Moreover, we notice that the performance of the Robin–Robin schemes with interface parameters provided by the 3D-cylindrical are always better than the one provided by the classical Dirichlet–Neumann scheme with Aitken procedure, the computational effort being reduced of about two times for $H_s = 0.005$ and more than three times for $H_s = 0.001$. This suggests that the cylindrical analysis and optimization could in general improve the efficiency of the Robin–Robin scheme for the FSI problem in haemodynamics.

6.3 Carotid simulation

In this section we report the numerical results obtained in a real geometry, namely a human carotid, see Fig. 8. The fluid mesh is composed by 9,655 vertices and 51,173 tetrahedra, corresponding to 80,138 degrees of freedom for the velocity and 9,655 for the pressure, whereas the structure mesh is composed by 11,052 vertices corresponding to 33,156 degrees of freedom for the structure displacement.

Table 2 Values of the optimized interface parameters and of (49), average number of iterations per time step, and normalized CPU time (computed with respect to the best performance for each row)

$H_s - \gamma_{ST}$	2D/flat			3D/cyl			DN-Aitken	
	σ_f/σ_s	# Iter	CPU time	σ_f/σ_s	# Iter	CPU time	# Iter	CPU time
$0.001–1.5 \times 10^7$	318,900/−16,000	5.7	1.3	225,000/−66,400	4.9	1.0	18.3	3.6
$0.001–3.0 \times 10^7$	468,900/−16,000	6.7	1.5	337,500/−72,900	4.6	1.0	16.0	3.2
$0.005–1.5 \times 10^7$	994,600/−16,000	24.6	3.7	325,000/−152,200	6.3	1.0	13.8	2.0
$0.005–3.0 \times 10^7$	114,4600/−16,000	21.5	3.0	375,000/−173,400	6.4	1.0	13.1	1.9

In the last columns we reported the Dirichlet–Neumann case. Cylindrical simulation

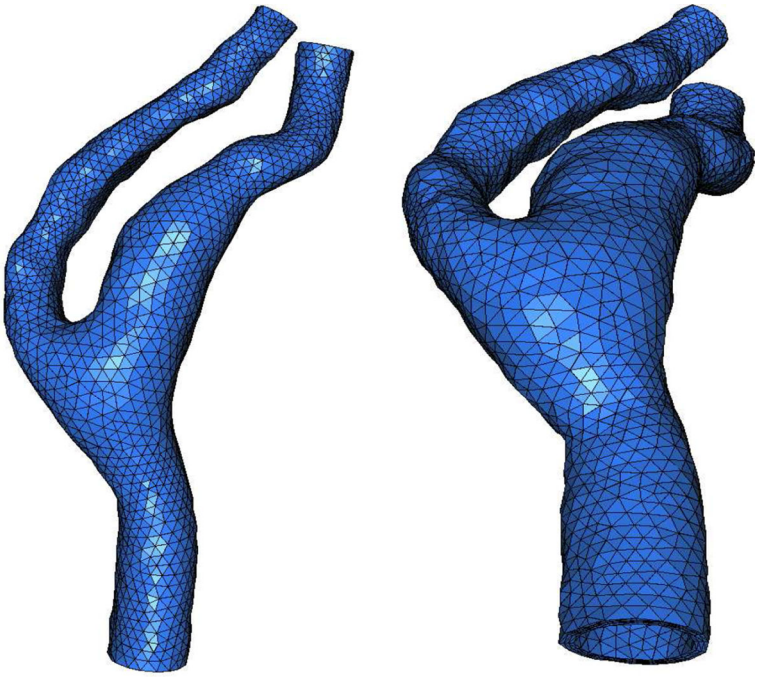

Fig. 8 Carotid fluid (*left*) and structure (*right*) computational domains. The fluid domain has been reconstructed from MRI images (courtesy of Dr. M. Domanin, Fondazione IRCSS Cà Granda, Ospedale Maggiore Policlinico, Milan, Italy), whereas the structure domain has been obtained by extrusion of the fluid one

In this case the values of the radius and of the wall thickness to be used to obtain the estimates provided by Theorem 2 are not defined uniquely. For this reason, we needed to consider representative radius and wall thickness values. To this aim, we considered three scenarios obtained by taking these values at the inlet, at a section belonging to the internal carotid (ICA) just below the bifurcation, and at the ICA outlet. Moreover, we set $\gamma_{ST} = 3 \times 10^7$ Pa/m, the frequencies vary in the ranges $m = 0, \ldots, m_{max}$ (with m_{max} depending on the chosen radius) and $70 \leq k \leq 4,200\,\mathrm{m}^{-1}$. In Table 3 we reported the values of m_{max}, $\overline{M}$, ρ_0 and of the optimal range of p provided by the estimates in Theorem 2 for the three selected scenarios.

We ran the simulations with different values of p within the three estimated ranges. In Fig. 9 we reported the fluid pressure in the deformed domain at four different instants, whereas in Table 4 we show the performance in terms of average number of iterations per time steps and CPU times for the three selected scenarios and for the DN scheme with Aitken relaxation procedure.

From these results we can see that the estimates provided by Theorem 2 are robust with respect to the choice of the carotid radius and thickness, the performance being quite independent of these values. Moreover, we observe in any case a reduction of the computational effort with respect to the Dirichlet–Neumann scheme with Aitken relaxation procedure, the mean number of iterations per time step and the CPU time being nearly halved. These results confirmed the suitability of the Robin–Robin scheme in

Table 3 Values of m_{max} , M, $\overline{\rho_0}$ and of the optimal range of p provided by the estimates in Theorem 2 for three different choices of the representative radius and wall thickness

	R	H_s	m_{max}	$\overline{M}$	ρ_0	$p \in$
Inlet	0.0024	0.00057	19	154,400	0.56	[198,100, 1,503,400]
ICA bifurcation	0.0034	0.00079	30	144,900	0.58	[183,000, 1,487,300]
ICA outlet	0.0018	0.00041	16	160,600	0.56	[204,800, 1,642,700]

Carotid simulation

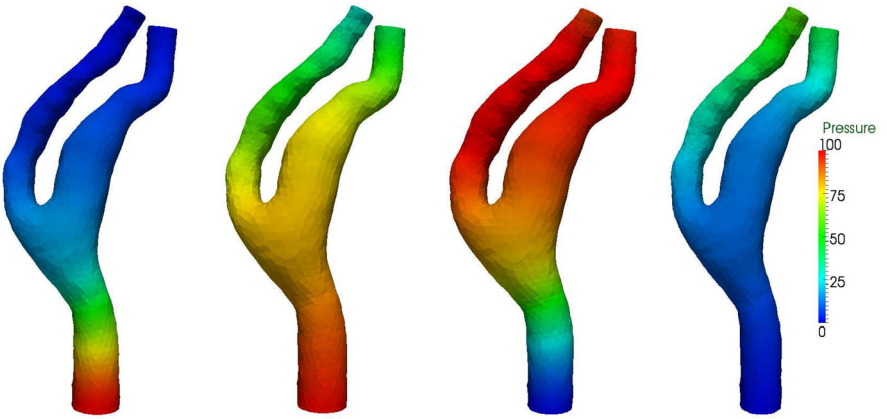

Fig. 9 Fluid pressure wave traveling along the deformed carotid domain. From *left* to *right*, we have $t = 0.001$ s, $t = 0.005$ s, $t = 0.010$ s, $t = 0.015$ s

Table 4 Values of the optimized interface parameters, average number of iterations per time step, and normalized CPU time, for different values of the representative carotid radius and thickness

	σ_f/σ_s	# Iter	CPU time
Inlet	437,500/−128,700	12.5	1.1
ICA bifurcation	425,000/−135,100	13.0	1.1
ICA outlet	450,000/−128,800	12.0	1.0
DN-Aitken	$+\infty/0$	24.3	1.9

In the last row the Dirichlet–Neumann case is reported. Carotid simulation

real haemodynamic application and the effectiveness of the estimates provided by Theorem 2.

Acknowledgments Giacomo Gigante has been partially supported by the Italian PRIN 2010-2011 "Real and complex manifolds: geometry, topology and harmonic analysis". Christian Vergara has been partially supported by the Italian MIUR PRIN09 project no. 2009Y4RC3B_001.

References

1. Astorino, M., Chouly, F., Fernández, M.: Robin based semi-implicit coupling in fluid–structure interaction: stability analysis and numerics. SIAM J. Sci. Comput. **31**(6), 4041–4065 (2009)
2. Badia, S., Nobile, F., Vergara, C.: Fluid–structure partitioned procedures based on Robin transmission conditions. J. Comput. Phys. **227**, 7027–7051 (2008)
3. Badia, S., Nobile, F., Vergara, C.: Robin–Robin preconditioned Krylov methods for fluid–structure interaction problems. Comput. Methods Appl. Mech. Eng. **198**(33–36), 2768–2784 (2009)
4. Badia, S., Quaini, A., Quarteroni, A.: Splitting methods based on algebraic factorization for fluid–structure interaction. SIAM J. Sci. Comput. **30**(4), 1778–1805 (2008)
5. Causin, P., Gerbeau, J.F., Nobile, F.: Added-mass effect in the design of partitioned algorithms for fluid–structure problems. Comput. Methods Appl. Mech. Eng. **194**(42–44), 4506–4527 (2005)
6. Deparis, S., Discacciati, M., Fourestey, G., Quarteroni, A.: Fluid–structure algorithms based on Steklov–Poincaré operators. Comput. Methods Appl. Mech. Eng. **195**(41–43), 5797–5812 (2006)
7. Dolean, V., Gander, M.J., Gerardo Giorda, L.: Optimized Schwarz methods for Maxwell's equations. SIAM J. Sci. Comput. **31**(3), 2193–2213 (2009)
8. Donea, J.: An arbitrary Lagrangian–Eulerian finite element method for transient dynamic fluid–structure interaction. Comput. Methods Appl. Mech. Eng. **33**, 689–723 (1982)
9. Dubois, O.: Optimized Schwarz methods with Robin conditions for the advection–diffusion equation. In: Widlund, O.B., Keyes, D.E. (eds.) Domain Decomposition Methods in Science and Engineering XVI, pp. 181–188. Springer-Verlag, New York (2006)
10. Fernández, M.A., Gerbeau, J.F., Grandmont, C.: A projection semi-implicit scheme for the coupling of an elastic structure with an incompressible fluid. Int. J. Numer. Methods Eng. **69**(4), 794–821 (2007)
11. Folland, G.B.: Introduction to Partial Differential Equations. Princeton University Press, Princeton (1995)
12. Formaggia, L., Quarteroni, A., Veneziani, A. (eds.): Cardiovascular Mathematics-Modeling and Simulation of the Circulatory System. Springer, Milan (2009)
13. Formaggia, L., Quarteroni, A., Vergara, C.: On the physical consistency between three-dimensional and one-dimensional models in haemodynamics. J. Comput. Phys. **244**, 97–112 (2013)
14. Forster, C., Wall, W., Ramm, E.: Artificial added mass instabilities in sequential staggered coupling of nonlinear structures and incompressible viscous flow. Comput. Methods Appl. Mech. Eng. **196**(7), 1278–1293 (2007)
15. Gander, M.J.: Optimized Schwarz methods. SIAM J. Numer. Anal. **44**(2), 699–731 (2006)
16. Gander, M.J., Magoulès, F., Nataf, F.: Optimized Schwarz methods without overlap for the Helmholtz equation. SIAM J. Sci. Comput. **24**, 38–60 (2002)
17. Gerardo Giorda, L., Nobile, F., Vergara, C.: Analysis and optimization of Robin–Robin partitioned procedures in fluid–structure interaction problems. SIAM J. Numer. Anal. **48**(6), 2091–2116 (2010)
18. Gigante, G., Pozzoli, M., Vergara, C.: Optimized Schwarz methods for the diffusion–reaction problem with cylindrical interfaces. SIAM J. Numer. Anal. **51**(6), 3402–3430 (2013)
19. Hairer, E., Nørsett, S.P., Wanner, G.: Springer Series in Computational Mathematics. Solving ordinary differential equations: nonstiff problems. Springer, Berlin (1993)
20. Japhet, C.: Optimized Krylov–Ventcell method. Application to convection–diffusion problems. In: Bjorstad, P.E., Espedal, M.S., Keyes, D.E. (eds.) Proceedings of the Ninth International Conference on Domain Decomposition Methods, pp. 382–389 (1998)
21. Japhet, C., Nataf, N., Rogier, F.: The optimized order 2 method. Application to convection–diffusion problems. Fut. Gen. Comput. Syst. **18**, 17–30 (2001)
22. Küttler, U., Wall, W.A.: Fixed-point fluidstructure interaction solvers with dynamic relaxation. Comput. Mech. **43**(1), 61–72 (2008)
23. Lebedev, N.: Special Functions and Their Applications. Courier Dover Publications, New York (1972)
24. LifeV project: http://www.lifev.org (2004)
25. Lions, P.L.: On the Schwarz alternating method III. In: Chan, T., Glowinki, R., Periaux, J., Widlund, O.B. (eds.) Proceedings of the Third International Symposium on Domain Decomposition Methods for PDE's, pp. 202–223. SIAM, Philadelphia (1990)
26. Magoulès, F., Ivanyi, P., Topping, B.H.V.: Non-overlapping Schwarz method with optimized transmission conditions for the Helmholtz equation. Comput. Methods Appl. Mech. Eng. **193**, 4797–4818 (2004)

27. Moireau, P., Xiao, N., Astorino, M., Figueroa, C.A., Chapelle, D., Taylor, C.A., Gerbeau, J.-F.: External tissue support and fluidstructure simulation in blood flows. Biomech. Model. Mechanobiol. **11**(1–2), 1–18 (2012)
28. Nobile, F., Pozzoli, M., Vergara, C.: Time accurate partitioned algorithms for the solution of fluid–structure interaction problems in haemodynamics. Comput. Fluids **86**, 470–482 (2013)
29. Nobile, F., Pozzoli, M., Vergara, C.: J. Comput. Phys. **273**, 598–617 (2014)
30. Nobile, F., Vergara, C.: An effective fluid–structure interaction formulation for vascular dynamics by generalized Robin conditions. SIAM J. Sci. Comput. **30**(2), 731–763 (2008)
31. Nobile, F., Vergara, C.: Partitioned algorithms for fluid–structure interaction problems in haemodynamics. Milan J. Math. **80**(2), 443–467 (2012)
32. Qaddouria, A., Laayounib, L., Loiselc, S., Cotea, J., Gander, M.J.: Optimized Schwarz methods with an overset grid for the shallow-water equations: preliminary results. Appl. Numer. Math. **58**, 459–471 (2008)
33. Stupfel, B.: Improved transmission conditions for a one-dimensional domain decomposition method applied to the solution of the Helmhotz equation. J. Comput. Phys. **229**, 851–874 (2010)